

# ME525 Applied Acoustics Lecture 21, Winter 2022

## Working with ray theory

### Introduction to waveguides

Peter H. Dahl, University of Washington

#### Simple, practical ray equations based on the linear sound speed gradient

Ray fans are "fans" of rays "launched" from a sound source location; each ray has a different ray launch (horizontal) angle  $\theta_0$ . Take the sound speed at the source location as  $c_0$ , then Snell's law dictates how the ray responds going forward from that point. In fact, the ratio  $\frac{\cos \theta_0}{c_0}$  will forever stick with that ray, and this value is known as the *ray parameter* for a given ray. Thus, were the sound speed to be constant, then the ray continues as a straight line, maintaining the initial launch angle  $\theta_0$ . If there is change in sound speed to  $c_1$  then Snell's law determines the new angle  $\theta_1$ , via  $\frac{\cos \theta_0}{c_0} = \frac{\cos \theta_1}{c_1}$ .

Ray fans give a useful qualitative view of how sound propagates away from a source, and show where shadow regions (where the density or concentration of rays is low), or convergence regions (density of rays is high). Figure 1 depicts a fan of rays emitted from a source at depth 40 m over a spread launch angles of  $\pm 40^\circ$ , for conditions representing a summer sound speed profile off the coast of New England. At range  $\sim 150$  m, depth  $\sim 45$  m, there is lower density of rays, at range 200-300 m, depth  $\sim 20$  to 30 m, there is a higher density of rays, which influences the overall sound intensity received at these locations.

Observe that several rays, e.g.  $\sim$  at depth 10 m, range 200 m, have reached a horizontal angle of  $0^\circ$  and have turned around to eventually reflect from the sea bed. Upon reflection these rays will again reach precisely the same turn-around depth, e.g., some at about range 900 m, with process repeated. A group of such rays, all having similar turn-around depths and ranges, forms a feature known as a *caustic*, represented here as the darker curve developing at depth  $\sim 25$  m, between ranges 200-500 m.

## Ray Fan (specific receiver not identified)

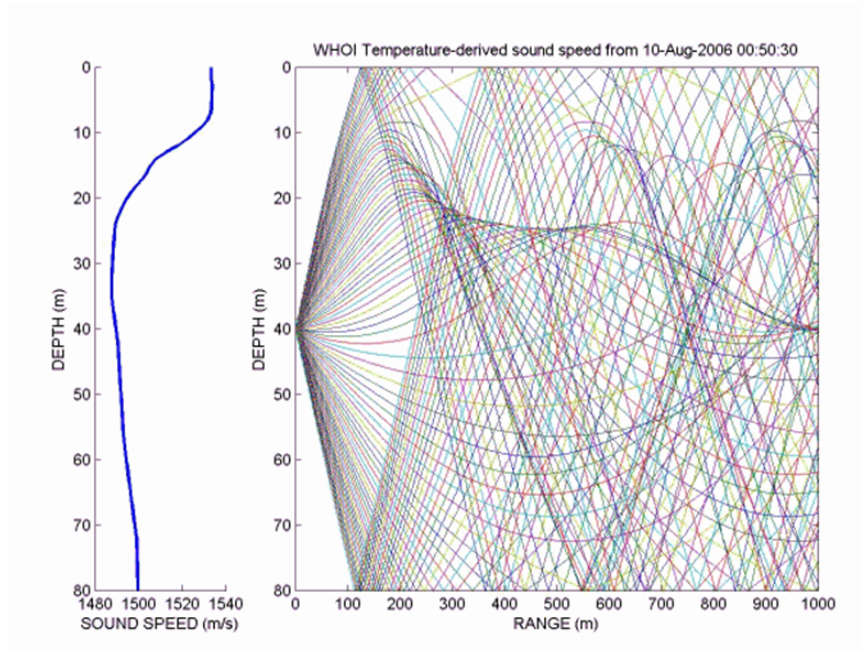


Figure 1: A fan of rays emitted from a source at depth 40 m over a launch angle spread of  $\pm 40^\circ$ , for conditions representing a summer sound speed profile of the coast of New England. At range  $\sim 150$  m, depth  $\sim 45$  m, there is lower density of rays, at range 200-300 m, depth  $\sim 20$  to 30 m, there is a higher density of rays, which influences the overall sound intensity received at these locations.

## Eigenrays (specific receiver identified)

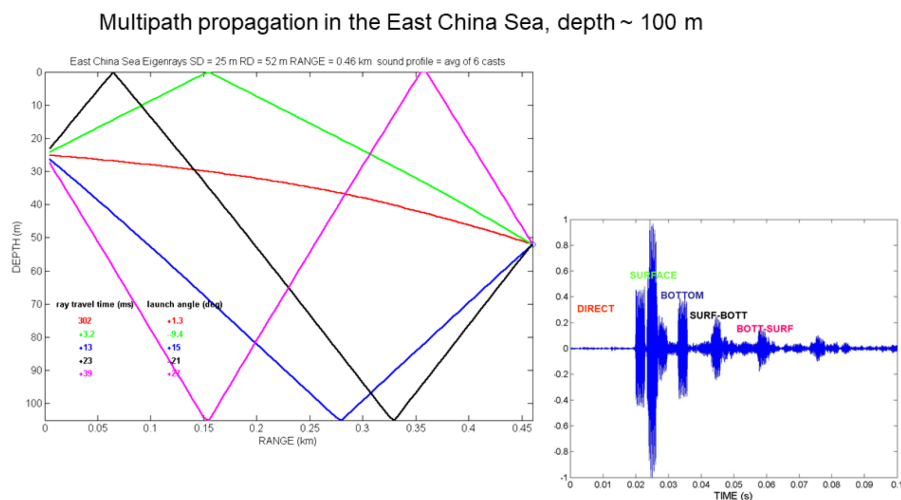


Figure 2: Multipath propagation in the East China Sea. The direct path with launch angle  $+1.3^\circ$  and having no reflections reached the receiver down range at 0.46 km, in 302 ms. The path reflecting first from the seabed then from the sea surface with launch angle  $+27^\circ$  reaches the receiver 39 ms later. This is well predicted by ray theory as shown by the data in lower right (time axis is relative).

Eigenrays are often used for more quantitative information, such as finding the arrival time for a particular ray. In underwater acoustics (as with many other applications in acoustics) sound from source reaches a receiver via multiple pathways. Figure 2 shows what is known as multipath propagation, this example is from measurements made in East China Sea. The direct path with launch angle  $+1.3^\circ$  and having no reflections reached the receiver down range at 0.46 km, in 302 ms. The path reflecting first from the seabed then from the sea surface with launch angle  $+27^\circ$  reaches the receiver 39 ms later. This is well predicted by ray theory as shown by the data in lower right (time axis is relative).

Eigenrays are the subset of rays in the ray fan that reach a specific receiving location. Finding eigenrays is necessarily achieved in some approximate sense, by finding a ray that reached depth  $z \pm \Delta z$  and range  $r \pm \Delta r$ , where one experiments with  $\Delta z, \Delta r$  until a suitable result found. The eigenray problem is somewhat more difficult because of this optimization task, but computation of ray fans or eigenrays is still relatively straight forward. A good starting guide is the monograph by Hovem (2013), which you can download for free.

However, we can make considerable quick progress with ray theory assuming the sound speed  $c$  varies in a linear manner with depth  $z$ , as in  $g = \frac{dc}{dz}$ . The key property in this case is that refraction will be manifested by rays following arcs of a circle, for which the radius of curvature goes as the inverse of the gradient  $g$ . (This should make sense intuitively: with no variation  $g = 0$  and radius of curvature is infinite, representing a straight line.) Figure 3 provides a set handy equations for ray travel time  $\Delta T$ , radius of curvature  $R_c$ , change in range  $\Delta R$  and change in depth  $\Delta z$  for a linear sound speed gradient  $g$ .

### Example of linear sound speed approximations for ray theory applied to sound in air

An example of how one might use these linear profile ray equations comes from a problem we paraphrase from Garrett (2017). A highway engineer is tasked with measuring road noise at range 150 from the road. Data for sound speed at 0.5 m above ground (342.8 m/s) and at 5 m (341.3 m/s), indicates a more typical reduction in temperature with height above ground (i.e., not a temperature inversion), and from this data we estimate the gradient  $|g| = 0.333 \text{ s}^{-1}$ .

The objective is to measure the sound emerging from cars with launch angle  $0^\circ$  as caused by tire noise (the largest source of car noise). Given the sound speed data, the engineer knows that the  $0^\circ$  ray will refract upwards, towards the lower sound speed region. Thus how high above the ground should the microphone be placed at range 150 m to have a good measurement of sound that was emitted horizontally from tires?

The decreasing sound speed with height above ground means upward refracting rays will have a constant radius of curvature that goes as the inverse of the gradient  $g$  (Fig. 4), and a shadow zone along ground level will develop. We find  $R_c = |342.8/0.333| = 1029 \text{ m}$ , given the gradient estimate for  $g$  and that the initial launch angle  $0^\circ$ . The range  $\Delta R$  is established to be 150 m, which

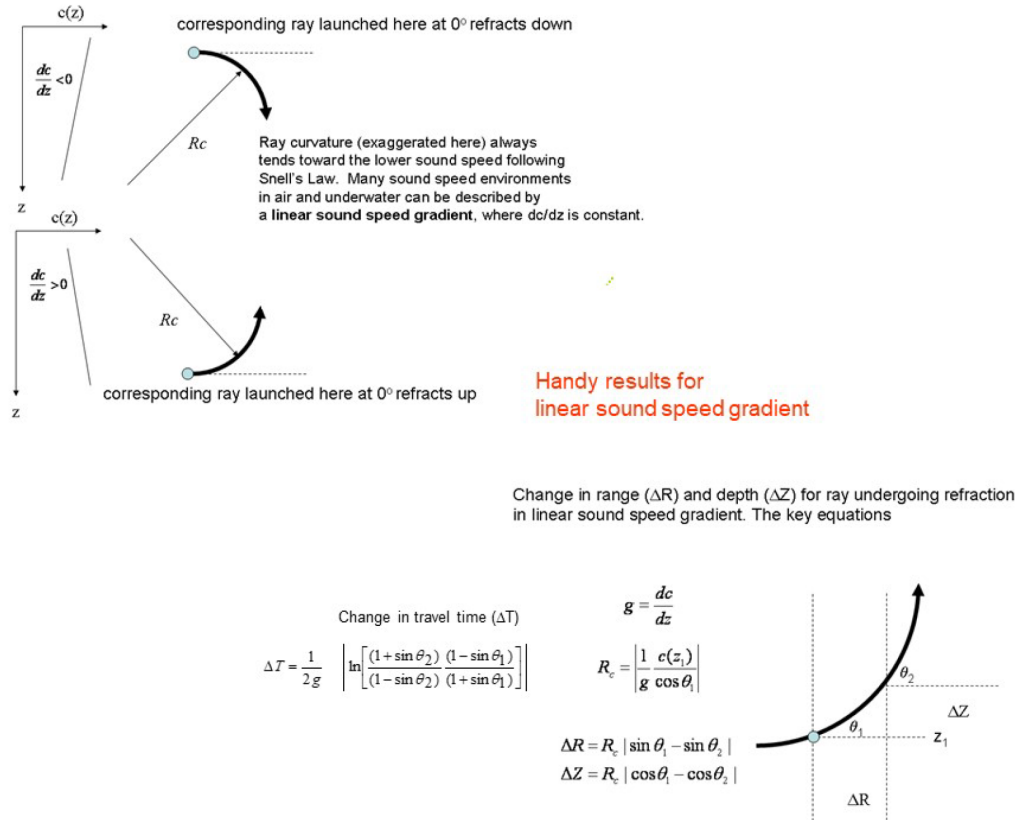


Figure 3: Refraction of rays with radius of curvature  $R_c$  due to propagation through a linear sound speed gradient, and handy set of equations for finding ray travel time  $\Delta T$ , radius of curvature, change in range  $\Delta R$  and change in depth  $\Delta z$  for a linear sound speed gradient  $g$ . Note: with  $g = \frac{dc}{dz}$  then  $g$  can be either negative or positive, so use  $|g|$  in the expressions for  $R_c$  and  $\Delta T$ .

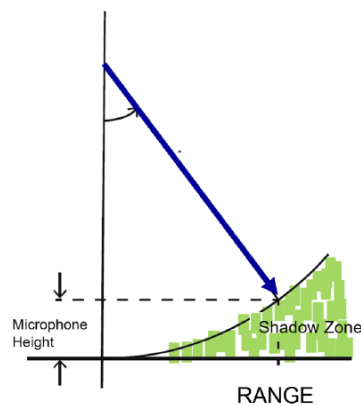


Figure 4: Shadow zone (colored region) for the horizontal ray caused by typical near-ground temperature gradient, and radius of curvature for this ray.

determines  $\theta_2$  as  $8.4^\circ$ . Thus, following equations in Fig. 3 we estimate the microphone height  $\Delta z$  should be about 11 m to avoid being placed within the shadow zone.

## Example of linear sound speed approximations for ray theory applied to underwater sound

Figure 5 represents two typical sound speed profiles that composed of linear gradients. Of course these are simple approximations to a measured sound speed versus depth  $c(z)$  but they nevertheless provide a useful guide. The high-latitude (arctic) profile starts at  $c(0) = 1440$  m/s and increases 80 m/s over the 5000 m depth, thus the gradient  $g = 0.016$  s<sup>-1</sup>. You should understand that *any* ray launched will be upward refracting. The less saline near-surface melt-water produces the effect of a minimum sound speed near the sea surface.

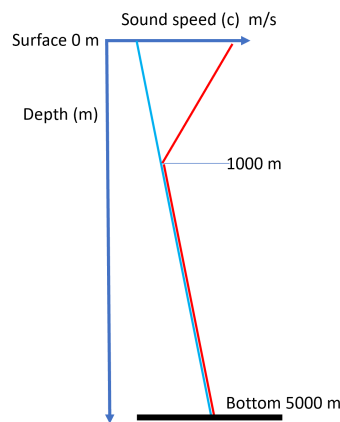


Figure 5: Underwater sound speed for arctic or high latitude (blue) and mid-latitude waters (red)

The mid-latitude profile has  $c(0) = 1490$  m/s, and decreases linearly to  $c(1000) = 1456$  m/s, thus the gradient  $g = 0.034$  s<sup>-1</sup>, after 1000 m the  $c(z)$  continues to increase with  $g = 0.016$  s<sup>-1</sup>. The decrease in speed from the surface to 1000 m is due to a *thermocline*, the increase thereafter at rate  $g = 0.016$  is the result of increasing hydrostatic pressure. You should memorize: underwater, the sound speed increases with increasing hydrostatic pressure, temperature and salinity. Because hydrostatic pressure is a known, constant effect, and salinity tends to vary a small about its nominal oceanic value, it is the temperature profile then that will often determine  $c(z)$ . Expendable bathythermographs (XBT) are often used by oceanographers and the navy for quick way to get the ocean temperature profile and hence sound speed. The final result for sound speed  $c(z)$  requires use of one of the many empirical equations. A simple one is (Medwin and Clay):

$$c = 1449.2 + 4.6T - 0.055T^2 + 0.00029T^3 + (1.34 - 0.01T)(S - 35) + 0.016z \quad (1)$$

In the next lecture we'll take the profile in Fig. 5 and trace out a few rays by hand. There is also a monograph on our website "High Frequency Underwater Sound" which you should download for more perspective on ray theory.

## Introduction to waveguides

By now we should have a pretty good sense that a sound source placed in environment without any confining boundaries, will have a pressure amplitude that reduces with range  $R$  from that source, going as  $1/R$ . This is known as spherical spreading. For example, this is demonstrated with the generalized model for point source at position vector  $\vec{r}_0$ , and receiver point a position vector  $\vec{r}$  defining  $R = |\vec{r} - \vec{r}_0|$ , such that

$$g = \frac{e^{ikR}}{4\pi R} \quad (2)$$

calling  $g$  the *free space* Green's function, which applied to an *unbounded* medium.

A waveguide is any kind of geometry, such as the confines of a stair well, or sound speed profile, or combination of these effects, which causes the sound pressure field to decay with range at a rate that is less than spherical spreading  $1/R$ . For example, in an underwater acoustic waveguide where geometry is constrained by the air water interface from above, and the seabed from below, the acoustic pressure field can decay as  $1/\sqrt{R}$  allowing for possibility of sound traveling considerably farther. In Fig. 1 there is waveguide effect owing to the confining property of sea surface and seabed boundaries, and a focusing property of the sound speed profile that tends to concentrate rays at depths associated with the minimum sound speed.

## References

- J. Hovem, Chapter: Ray Trace Modeling of Underwater Sound Propagation, In: *Modeling and Measurement Methods for Acoustic Waves and for Acoustic Microdevices*, 2013, Open Access via: DOI: 10.5772/55935
- H. Medwin and C. S. Clay *Fundamentals of Acoustical Oceanography*, (Academic Press, San Diego, CA, 1998)
- S. L. Garrett, *Understanding Acoustics*, (Springer, Acoustical Society of America Press, 2017).

# ME525 Applied Acoustics Lecture 22, Winter 2022

## More on ray theory and relation to waveguides

Peter H. Dahl, University of Washington

### More on practical ray equations based on the linear sound speed gradient

Let's continue with the two typical sound speed profiles that can be described (approximately) linear gradients (Fig. 1). The high-latitude (arctic) profile starts at  $c(0) = 1440$  m/s and increases 80 m/s over the 5000 m depth, thus the gradient  $g = 0.016$  s<sup>-1</sup>. The mid-latitude profile has  $c(0) = 1490$  m/s, and decreases linearly to  $c(1000) = 1456$  m/s, thus the gradient  $g = 0.034$  s<sup>-1</sup>, after 1000 m the  $c(z)$  continues to increase with  $g = 0.016$  s<sup>-1</sup>. The decrease in speed from the surface to 1000 m is due to a *thermocline*, the increase thereafter at rate  $g = 0.016$  is the result of increasing hydrostatic pressure.

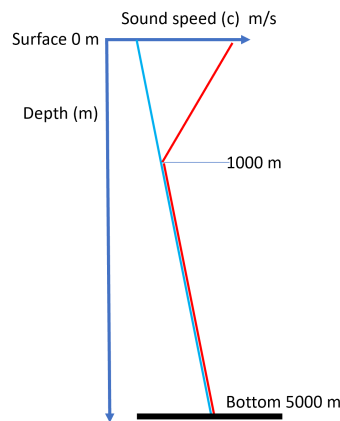


Figure 1: Underwater sound speed for arctic or high latitude (blue) and mid-latitude waters (red)

Suppose we had sonar system at depth 500 m, and wanted to launch a ray in waters described by the high-latitude (arctic) case, and this ray is to remain completely in the water column, i.e., does not undergo reflection from the seabed which can result in energy loss particularly if the grazing angle is greater than the critical angle. To cover the entire depth and also avoid reflection from the seabed, ray must reach a vertex point at or near the seabed. In other words we want the ray to have reached a grazing angle of  $0^\circ$  at (or near) the seabed, where the sound speed there, call it  $c_v$  equals 1520 m/s. What is the launch angle for this ray? At depth 500 m the sound speed  $c$  equals 1448 m/s; define this speed as  $c_0$ . Call the launch angle,  $\theta_v$  and find it directly from Snell's law:

$$\frac{\cos \theta_v}{c_0} = \frac{1}{c_v} \quad (1)$$

and equals  $17.7^\circ$ . From this we actually now that any ray with launch angle  $\pm 17.7^\circ$  will stay completely within the water column. For example, such information may serve as a design guide for sonar array for which the vertical angle is limited to  $\pm 18^\circ$ .

Such a ray will have a *cycle distance* – in this case the ray is directed towards the sea surface, reflect, then directed down to the vertex depth (about 5000 m), and refracts back up, repeat. We can find these distances in simple, approximate way as follows. Take the first segment from source depth 500 m to the surface. Find the radius of curvature  $R_c$  (refer to Fig. 3 of Lecture 21) where the applicable values are  $R_c = \left| \frac{1448}{g \cos 17.7^\circ} \right|$ , setting  $R_c$  to about 95 km. Next find  $\Delta R$  or the range from source at 500 m to the surface, where  $\Delta R = R_c |\sin 17.7^\circ - \sin 18.7^\circ|$  or about 1.6 km, and the  $18.7^\circ$  surface grazing angle is always found via Snell's law.

Next, at the surface this ray reflects and heads down to near the seabed, it will take another 1.6 km to get to the depth 500 m. After 500 m, it continues downward while continually lowering its grazing angle until vertex is reached. The range from depth 500 m to the vertex is found as  $\Delta R = R_c |\sin 17.7^\circ - \sin 0^\circ|$ , or about 29 km. Now another 29 km to arrive back at the depth 500 m, giving the cycle distance for this ray as 3.2 km plus 58 km or about 61 km. A ray fan for this profile (Fig. 2) shows the  $17.7^\circ$  ray (thick line) launched at depth 500 m with cycle distance nicely consistent with  $\sim 61$  km estimate made here by considerably simpler means.

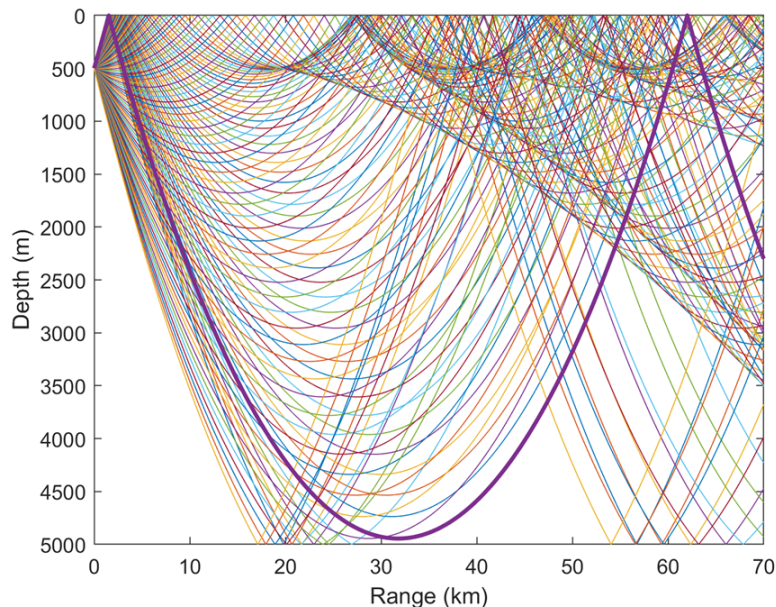


Figure 2: Ray fan and particular ray (thick line) launched at  $17.7^\circ$  at depth 500 m for the arctic or high latitude sound speed profile (Fig. 1). The cycle distance is  $\sim 61$  km.

Let's repeat the exercise using the mid-latitude case, again with a sonar system at depth 500 m with same goal of launching a ray that remains completely in the water column. In this case the sound speed at depth 500 m is  $c_0 = 1473$  m/s. The vertex speed  $c_v$  at depth 5000 m is also 1520

m/s, and from Snell's law we find  $\theta_v$  equal to  $14.3^\circ$ . Notice: this ray traversed two sound speed gradients to get to depth 5000 m, one downward-refracting and one upward refracting. Still, one simple Snell's law application gave us  $\theta_v$ .

This ray thus now refracts downward as it heads up toward the sea surface where the speed is 1490 m/s, and Snell's puts angle there at  $11.4^\circ$ . The  $R_c$  for this segment must take into account the higher gradient ( $g = 0.034$ ), with  $R_c = \left| \frac{1473}{g \cos 14.3^\circ} \right|$  equal to about 44.7 km. The range from source depth to surface is thus  $\Delta R = R_c |\sin 14.3^\circ - \sin 11.4^\circ|$  or about 2.2 km.

The ray reflects and takes another 2.2 km to get back to depth 500 m, where the grazing angle has again reached  $14.3^\circ$ . From there the ray must go another 500 m in depth after which the gradient of sound speed profile will change at depth 1000 m. The sound speed at 1000 m is 1456 m/s, so the ray must have reached a grazing angle of  $16.7^\circ$  (Snell's law), and the horizontal distance for this phase is  $\Delta R = R_c |\sin 14.3^\circ - \sin 16.7^\circ|$  or about 1.8 km.

From here the ray continues downward to the vertex depth of about 5000 m. The gradient has changed back to  $g = 0.016$  and  $R_c = \left| \frac{1456}{g \cos 16.7^\circ} \right|$  or about 95 km. Thus the range from depth 1000 m to 5000 m is  $\Delta R = R_c |\sin 16.7^\circ - \sin 0^\circ|$  or 27 km. Adding these ranges yields 4.4 km + 3.6 km + 54 km, or about 62 km. A ray fan for this profile (Fig. 3) shows the  $14.3^\circ$  ray (thick line) launched at depth 500 m with cycle distance also consistent with our simple estimate.

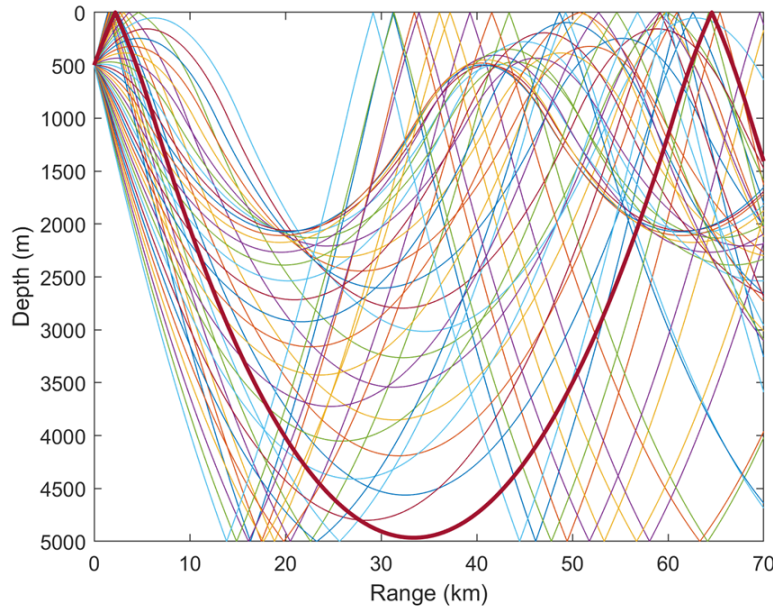


Figure 3: Ray fan and particular ray (thick line) launched at  $14.3^\circ$  at depth 500 m for the mid-latitude sound speed profile (Fig. 1). The cycle distance is  $\sim 62$  km. Notice the existence of caustics where ray converge, and shadow zones, where ray coverage is less.

Of course the sound speed profiles in Fig. 1 are idealized in two ways. The first being that sound speed  $c(z)$  can change both with range and time (more on time variation below), the second

being that water depth or bathymetry can change with range. Figure 4 illustrates this with data taken from the Marginal Ice Zone (MIZ). In the above two examples we have been studying *RSR paths* or a ray path that is refracted-surface-reflected, and our goal was to find the deepest RSR path. Additional, and more shallow, RSR paths are shown for the MIZ condition in Fig. 4.

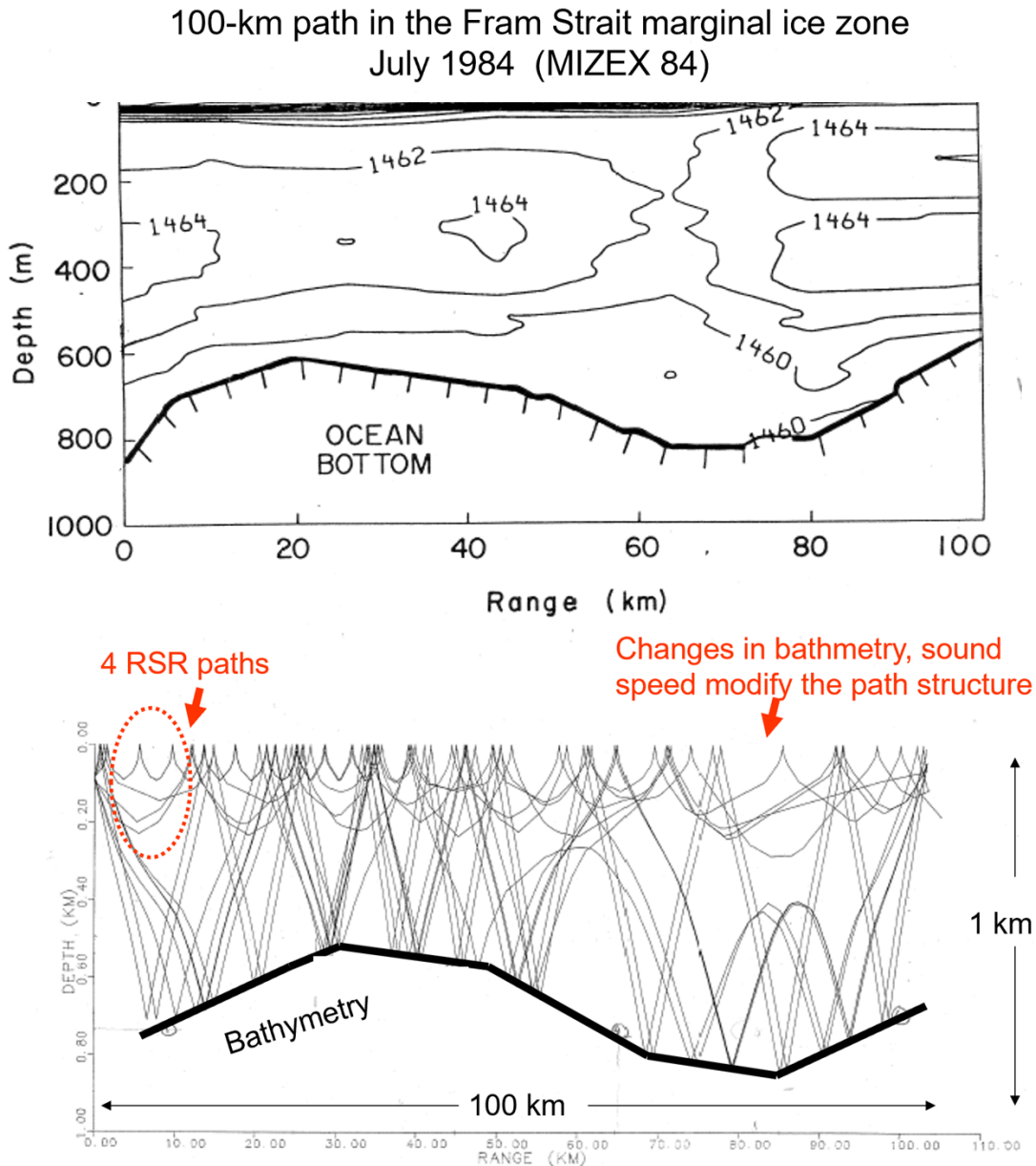


Figure 4: Top: Range-dependent bathymetry and sound speed profile over 100 km path in the Marginal Ice Zone. Figure from Dahl, Baggeroer, Mikhalevsky and Dyer, J. Acoust. Soc. Am., 1988. Not evident in the figure is the change in sound speed over the top 50-m from from about 1440 m/s to 1460 m/s. Bottom: rays computed for the above sound speed structure using a range-dependent ray trace program responsive to both changing depth and sound speed with range.

## Other examples of on use of ray theory

Figure 5 (left) conveys a variation in measured sound speed versus depth and time  $c(z; t)$  over a few hour period, with the largest variation occurring over the depth range 5 to 40 m as indicated by the gray shaded area. A set of eigenrays (right) for two receiver depths corresponding to  $c(z; t)$  shows the sensitivity of the eigenrays to such variation. Notice that the direct path eigenray to the more shallow receiver shows the most variation even though a surface reflected path traversed the same region of high sound speed variation. As a general rule, rays with lower grazing angle with respect to the horizontal as in this direct path ray, will be more sensitive to changes in sound speed.

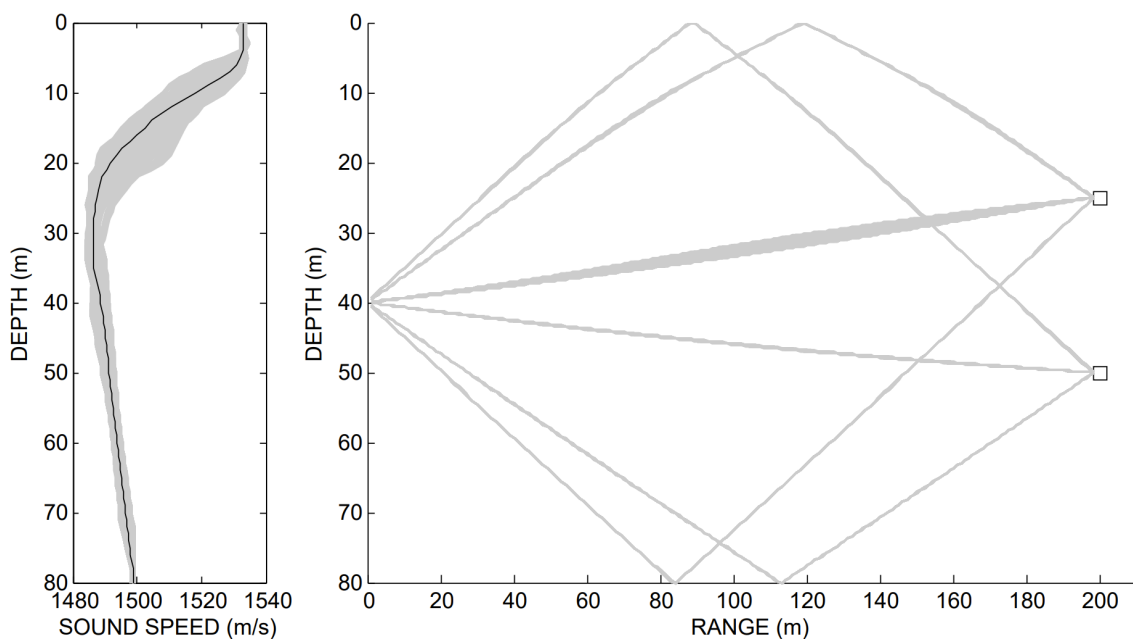


Figure 5: Left: Sound speed profile and typical variation over time due fluctuating oceanographic conditions. Right: Eigenrays computed for two receiver depths for spread of sound speed profiles. The direct path for the upper receiver is more sensitive to the fluctuating sound speed profile.

In Fig. 6, a simple demonstration of the effect of temperature inversion is shown for the case of hillside community and sound source below it. (This time of year temperature inversions are more frequent and you may on occasion experience more loudness from aircraft.) Ray theory provides an easy qualitative description of the effect of increasing sound speed with altitude owing to the inversion.

As a final example, although we generally think refraction as result of a change in sound speed with depth or altitude and use Snell's law to compute the change in ray angle, rays can also be refracted horizontally owing to large changes in bathymetry in the southern ocean. Figure 7 is from Dall'Osto (2019) showing likely propagation paths emerging from the explosion of the ARA San Juan submarine. The explosion was recorded at two Comprehensive Nuclear-Test-Ban Treaty

## Ray Theory for investigating community noise

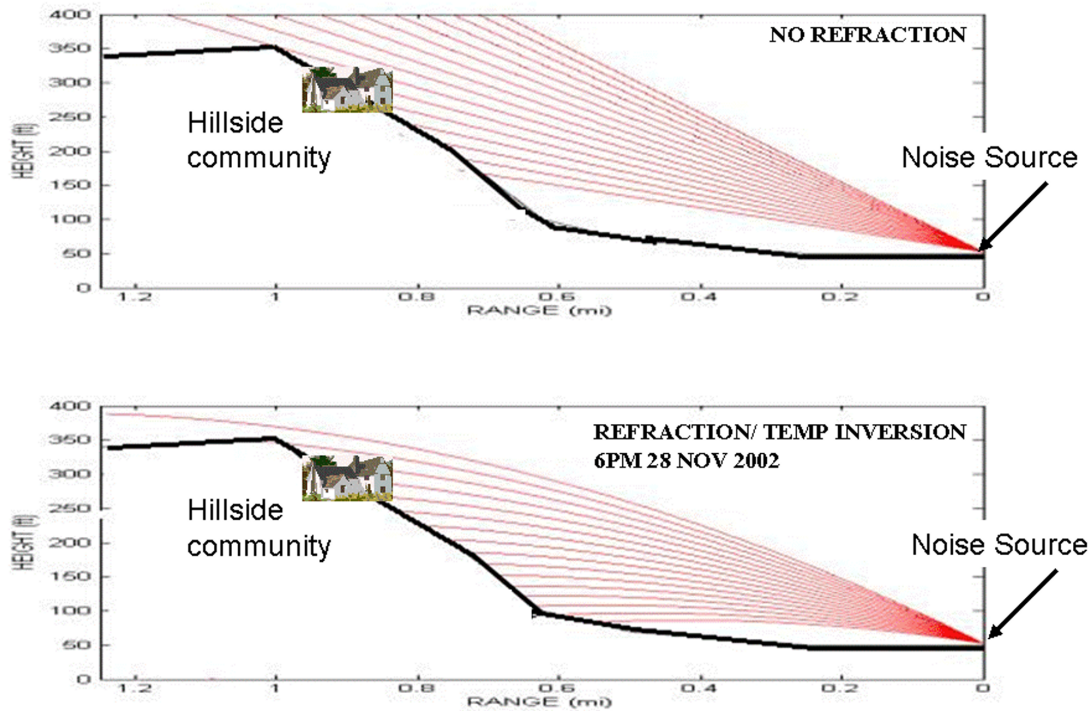


Figure 6: Top: sound rays emerging from a noise source traversing through air medium with constant sound speed. Bottom: temperature inversion causes sound speed to increase with altitude and rays from sound source are refracted downward; in this case the concentration of rays, hence loudness, at the hillside community has increased.

Organization (CTBTO) hydrophone listening stations, with data ultimately used to provide general a location where a search effort ensued.

This concludes our discussion of rays. If sound or acoustics is involved in your future career path, rays will invariably enter the picture. Likely you will not be writing your own complicated (and probably clunky) matlab program which I once did to make Figs. 2, 3 and 5 (I also produced Fig. 4 as a grad student but that was with a program from seismology) , but some aspect of refraction and rays will always be there. So, memorize Snell's law. We go on next to the formal underwater waveguide. Of course rays play a big part there but our focus for the remainder of the course will be on the method of normal modes.

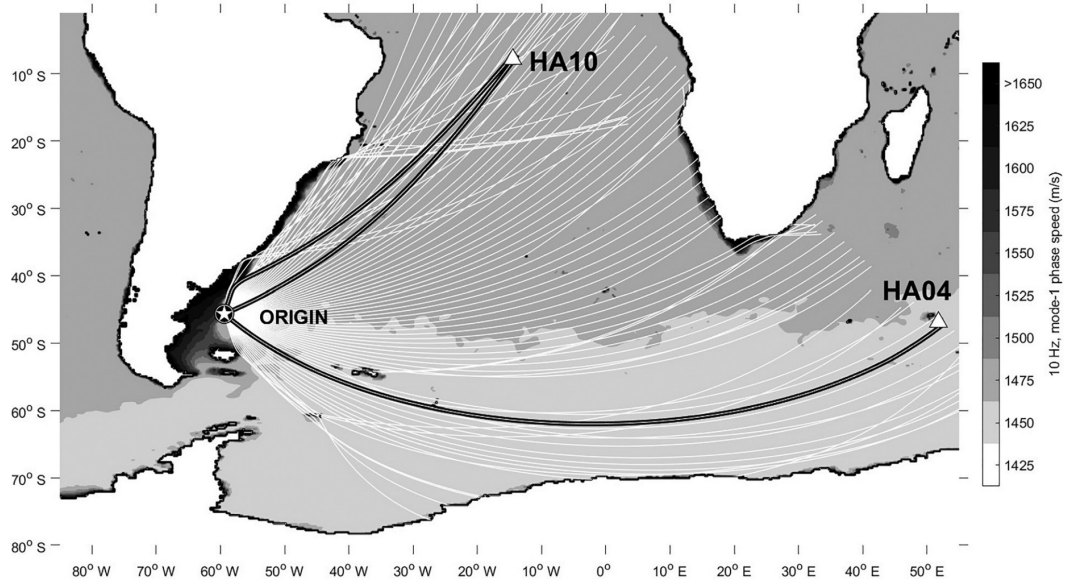


FIG. 1. Horizontal modal-eigenrays (thick black lines) representing 10-Hz mode-1 propagation paths from the origin  $46^{\circ}$  S,  $60^{\circ}$  W (star) to CTBTO hydroacoustic stations (triangles). A horizontal modal ray fan (white lines) shows effect of bathymetric refraction from the continental slope, caused by the rapid increase in phase speed (shaded contours).

Figure 7: Fig. 1 from Dall'Osto (2019), with original caption shown.

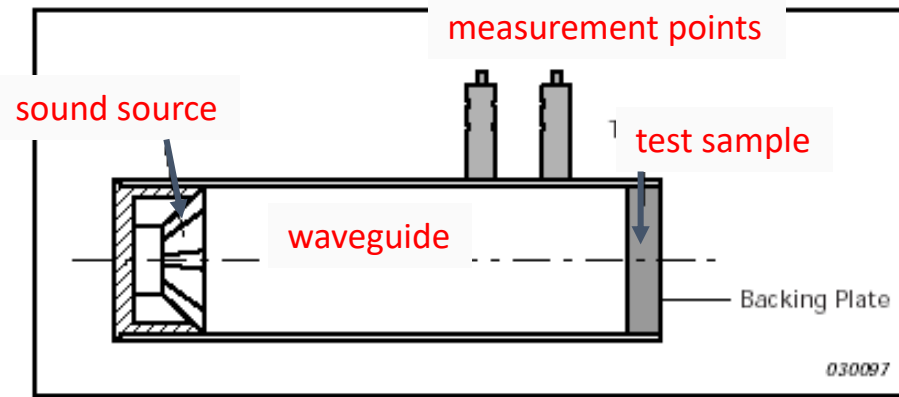
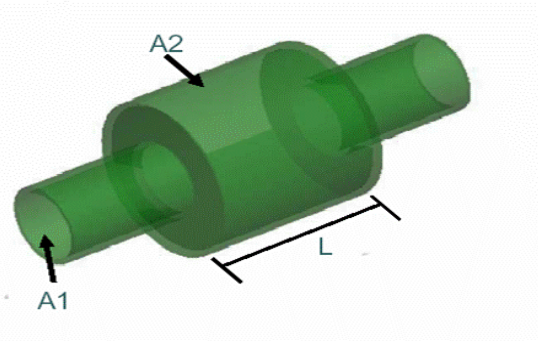
## References

D. R. Dall'Osto, "Source triangulation utilizing three-dimensional arrivals: Application to the search for the ARA San Juan submarine" *J. Acoust. Soc. Am.*, 146, Sep. 2019

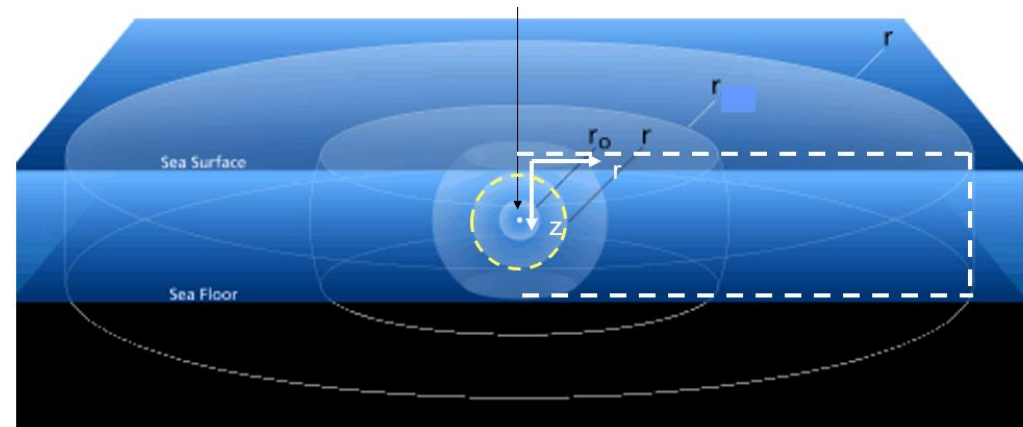
Acoustic waveguide:  
physical structure for guiding, or confining, sound waves.

(2) Impedance Tube for measuring acoustic properties of test sample

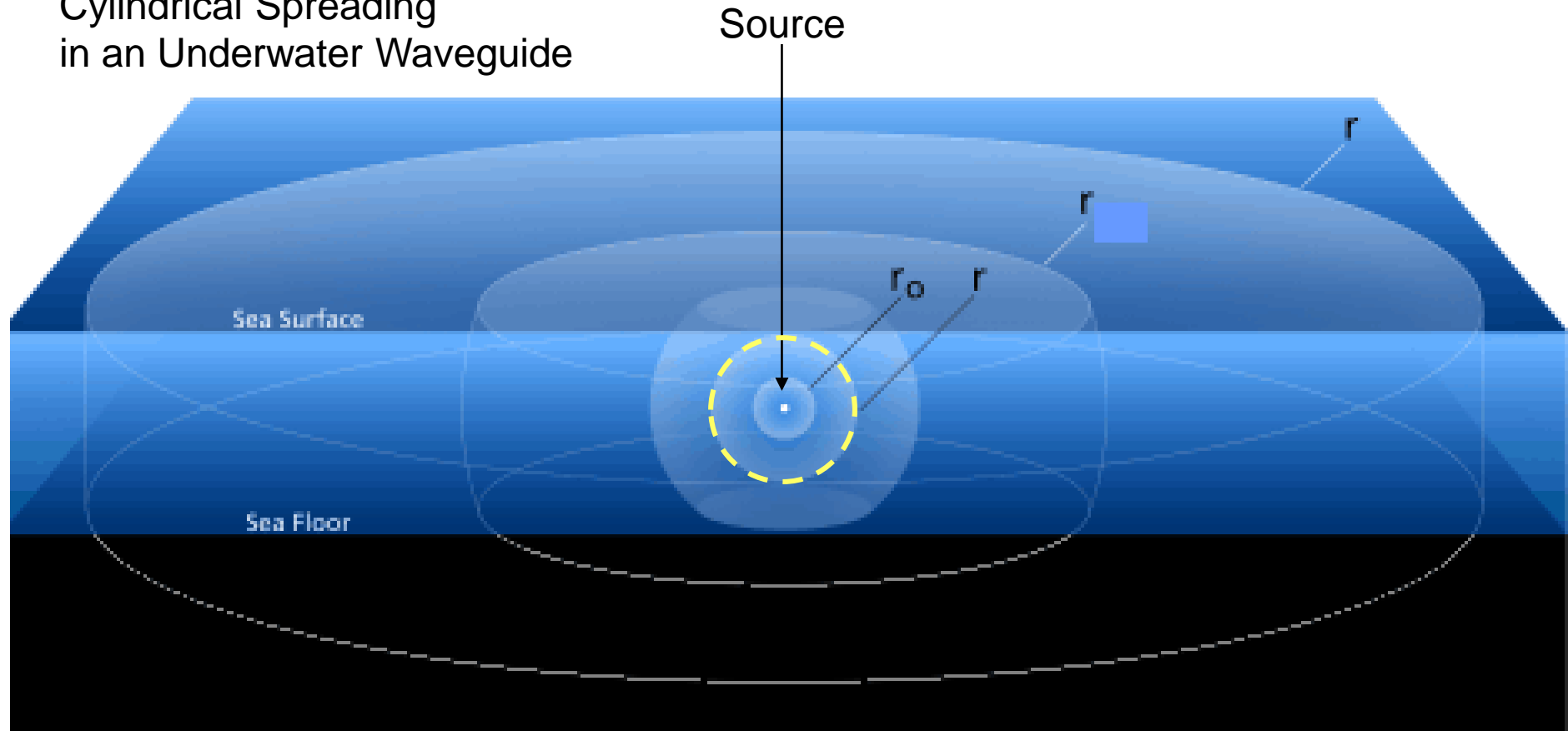
(1) Expansion Chamber (car exhaust muffler)



(3) Underwater acoustic waveguide



## Cylindrical Spreading in an Underwater Waveguide

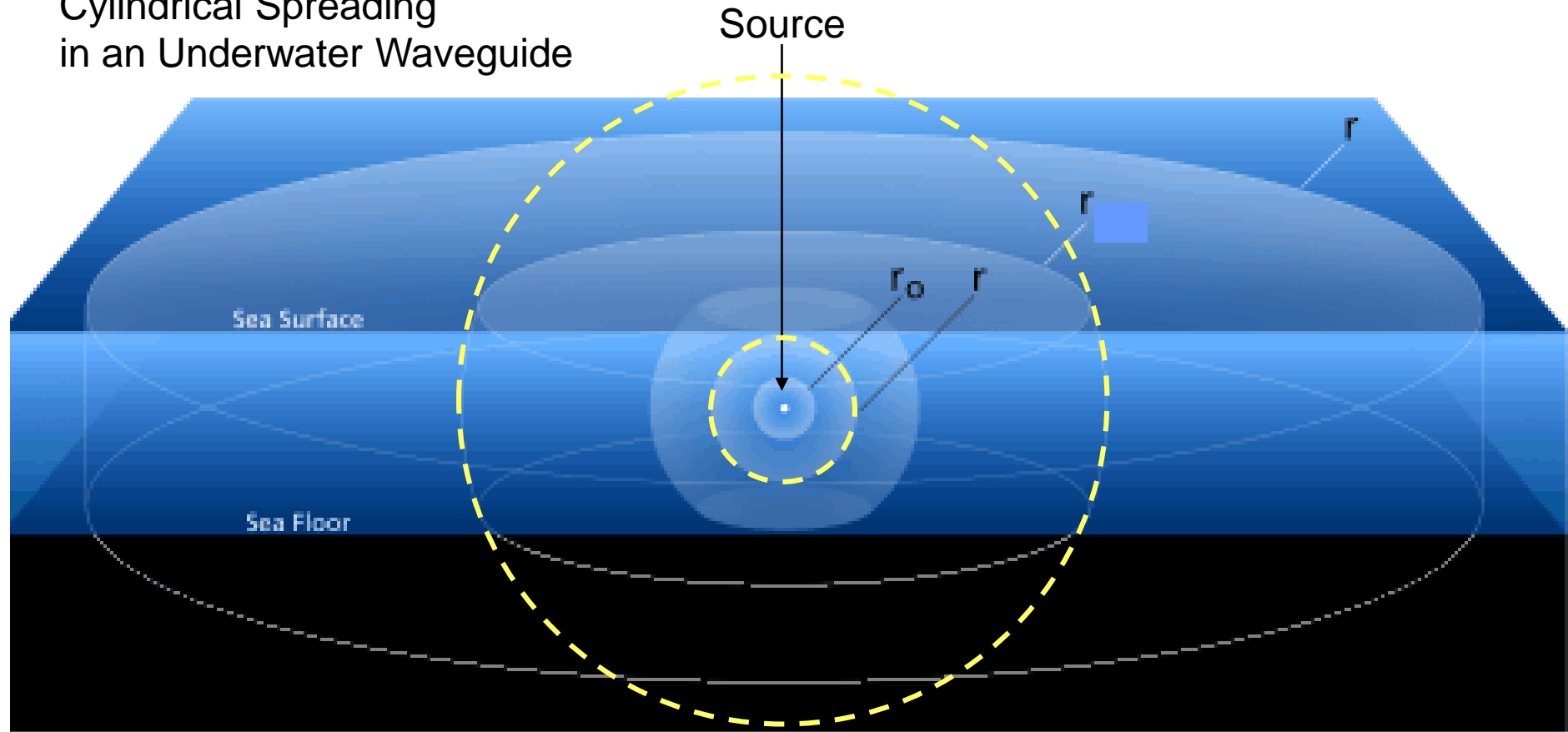


Between ranges  $r_0$  and  $r$  closest to source, (yellow circle)  
spreading follows a spherical law:

$$p \sim 1/r$$

:

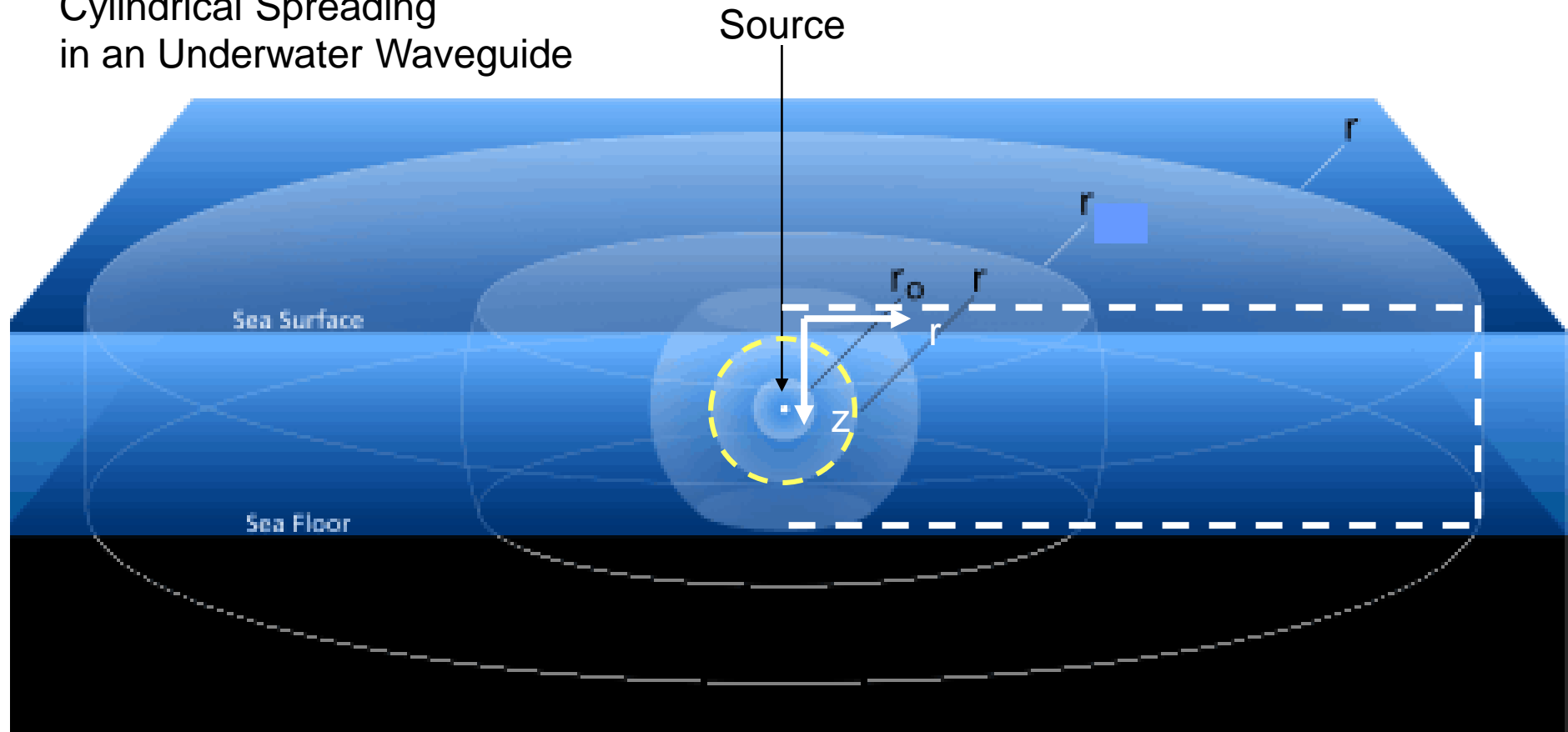
## Cylindrical Spreading in an Underwater Waveguide



Farther from source, the sphere is confined by sea surface and sea bed, spreading follows a cylindrical law:

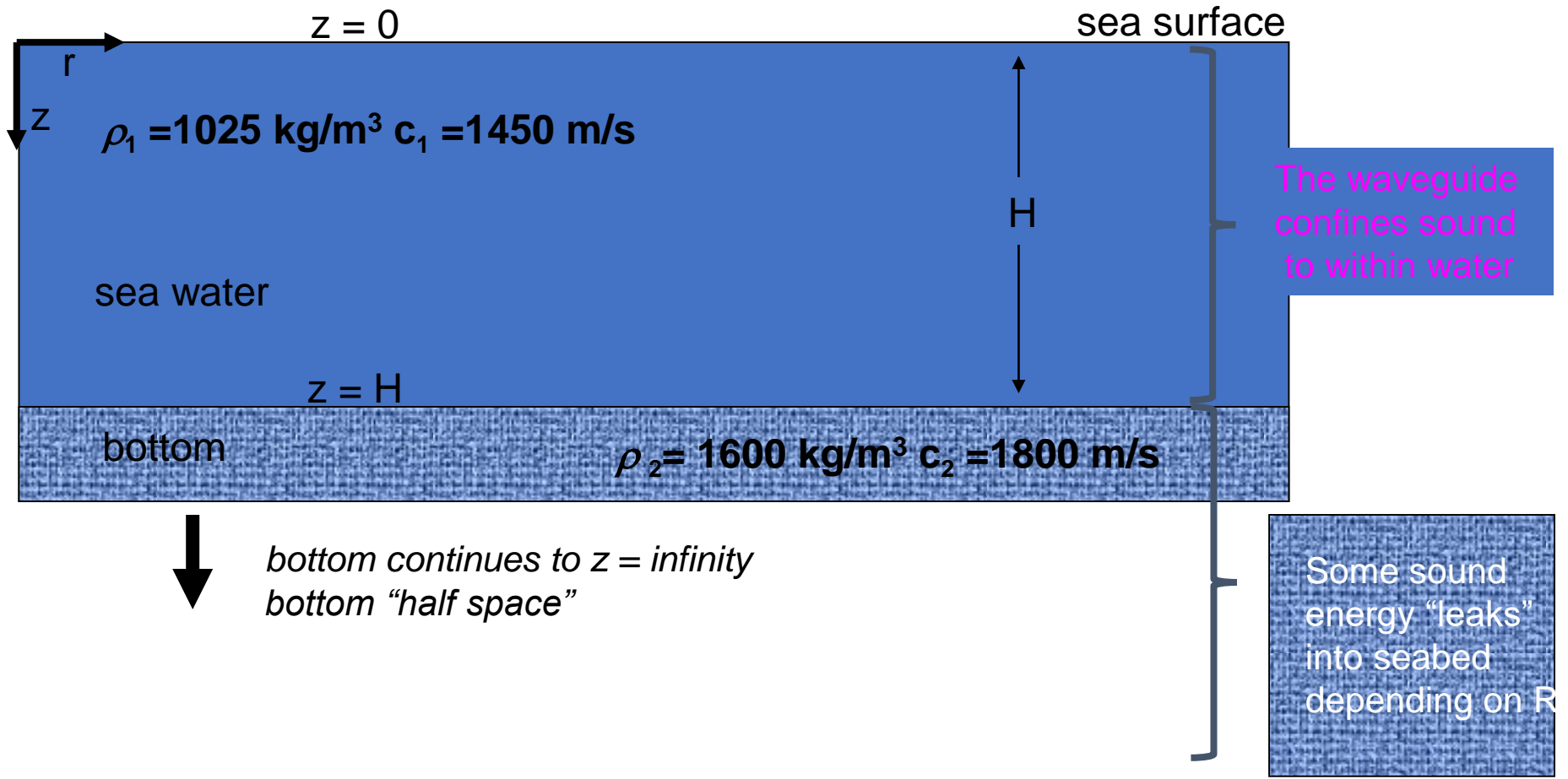
$$p \sim 1/\sqrt{r}$$

## Cylindrical Spreading in an Underwater Waveguide

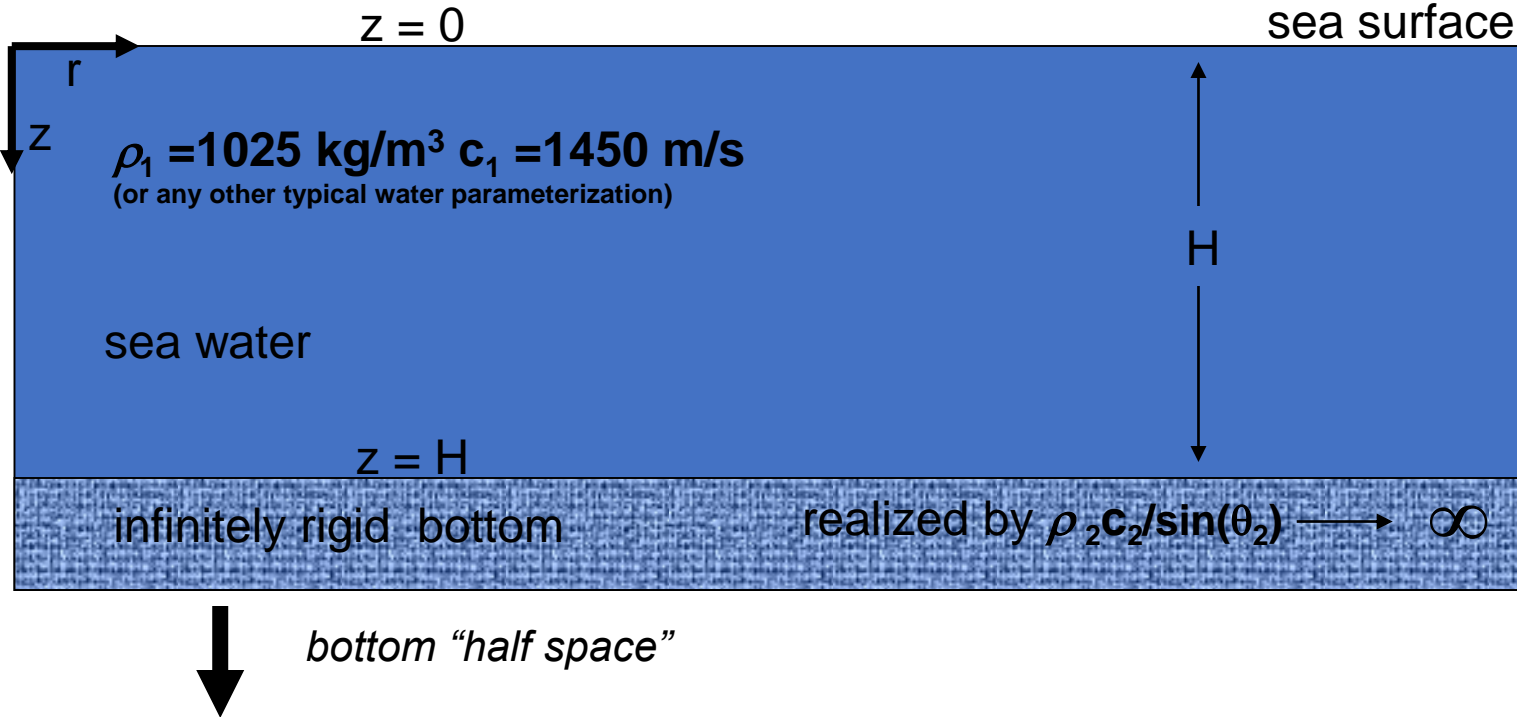


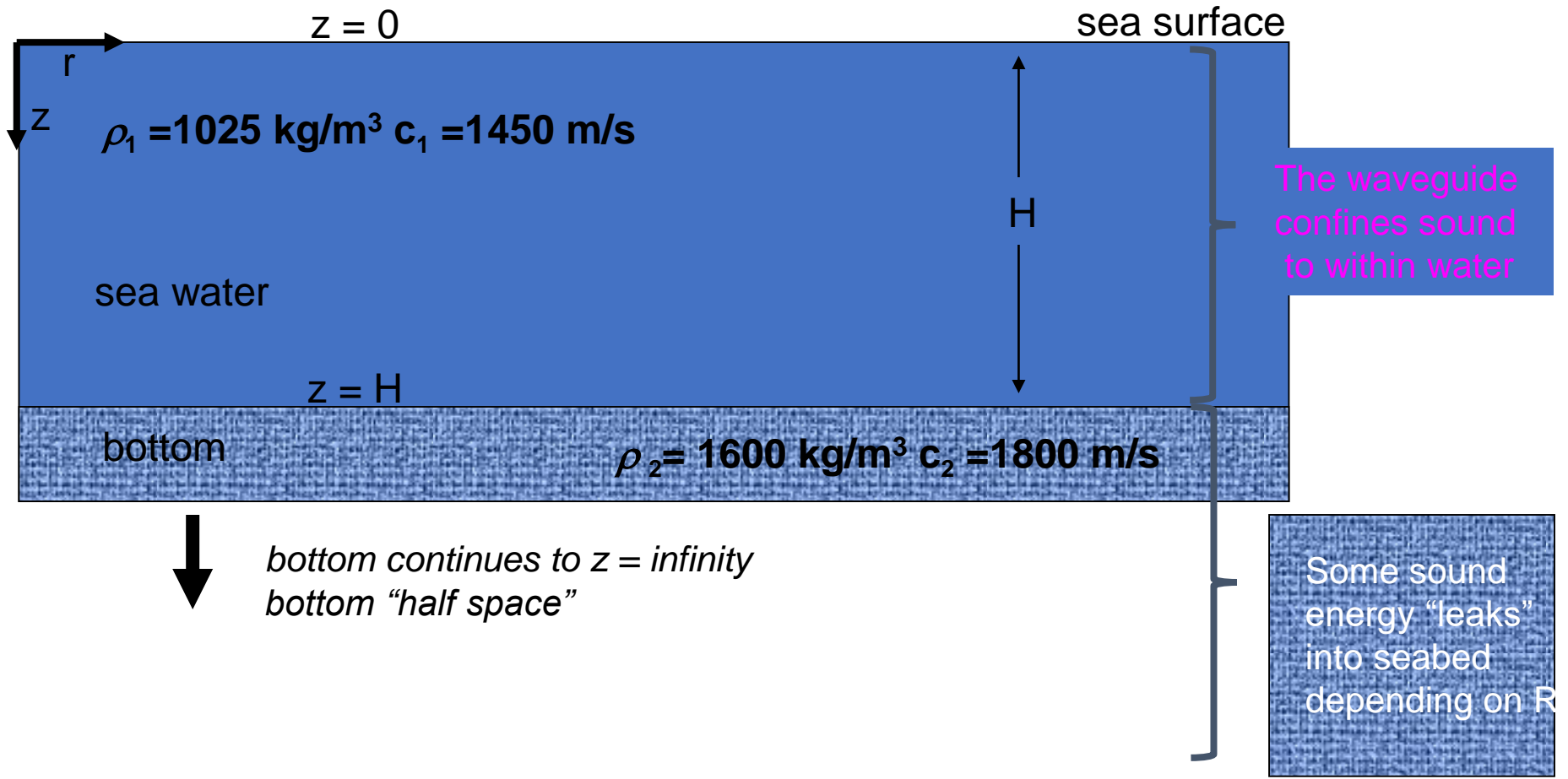
At any range  $r$ , the conditions are characterized by two spatial coordinates:  
 $r$  and  $z$ .

We study case for source at  $z = z_0$  and  $r = 0$ .

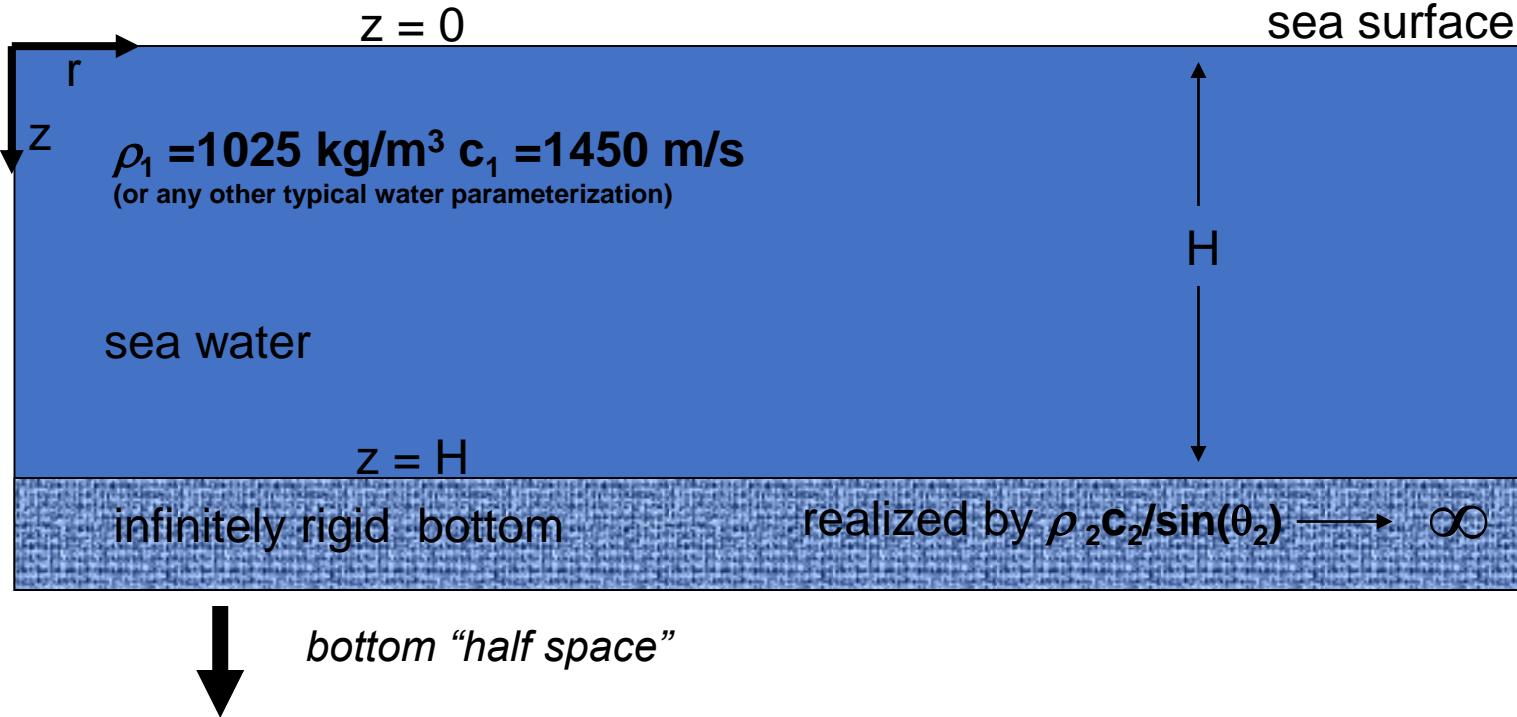


# Simple starting model for underwater waveguide





# Simple starting model for underwater waveguide

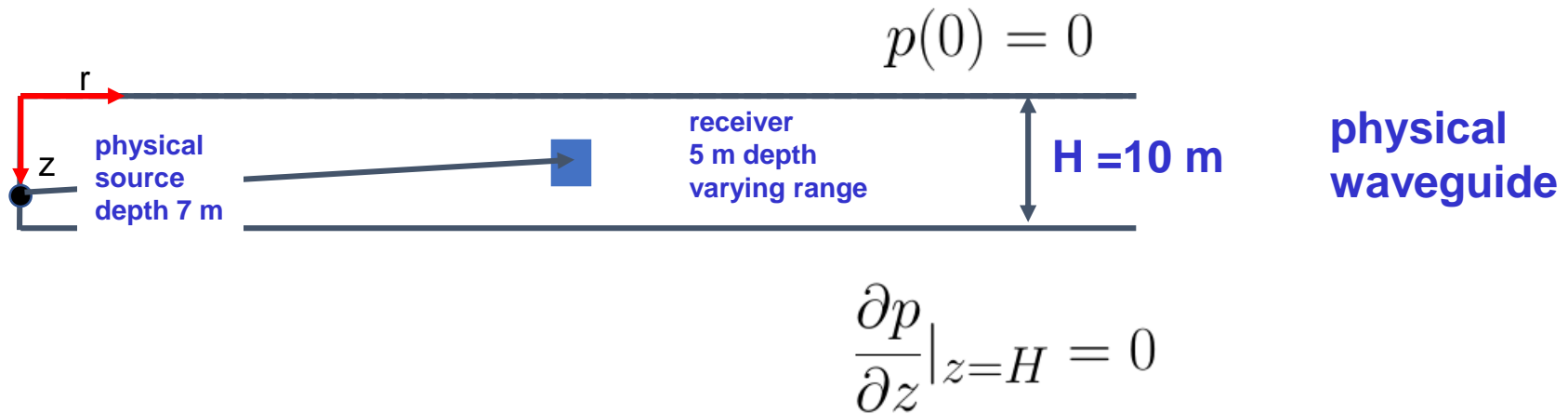


Method of Images solution of point source in an ideal waveguide

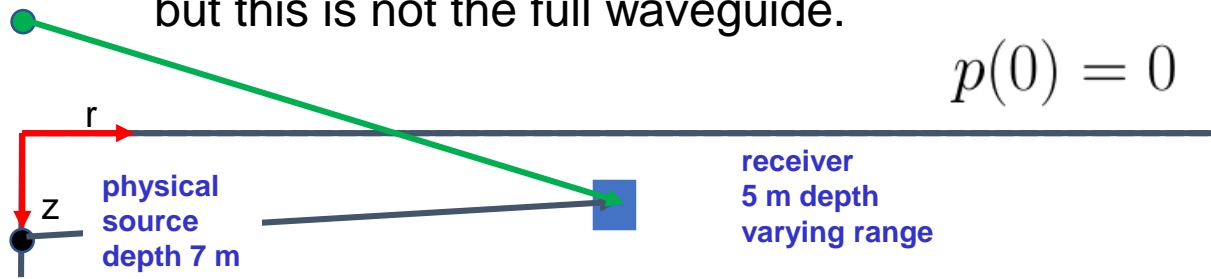
for which:

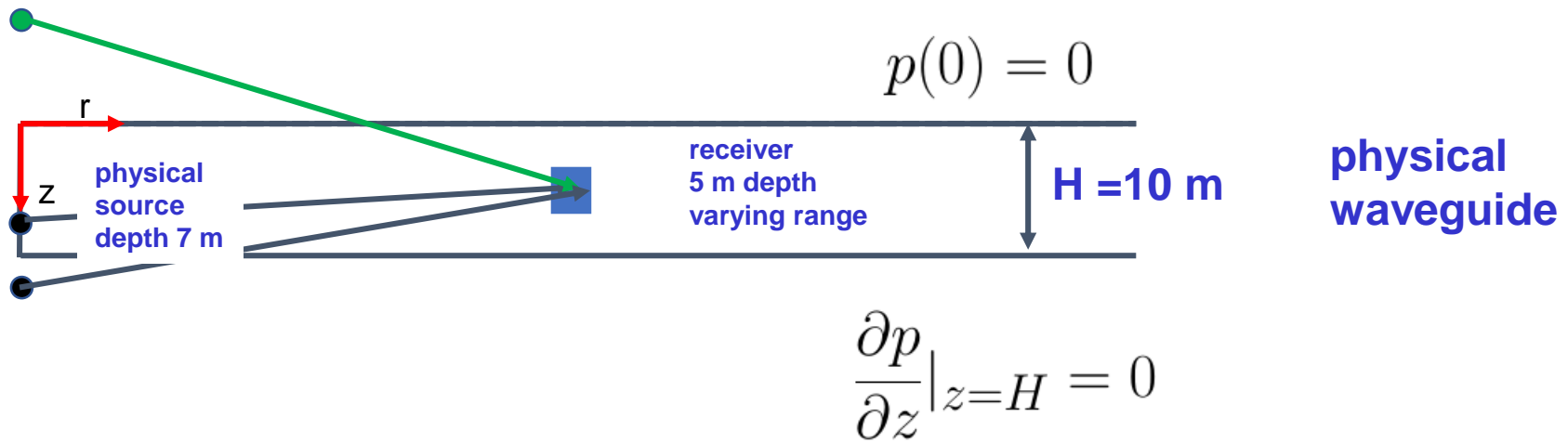
pressure = 0 at the air-water interface

and normal derivative pressure = 0 at  $z = H$



use negative image source to solve surface boundary condition (Lloyd Mirror problem). Already know this problem- but this is not the full waveguide.



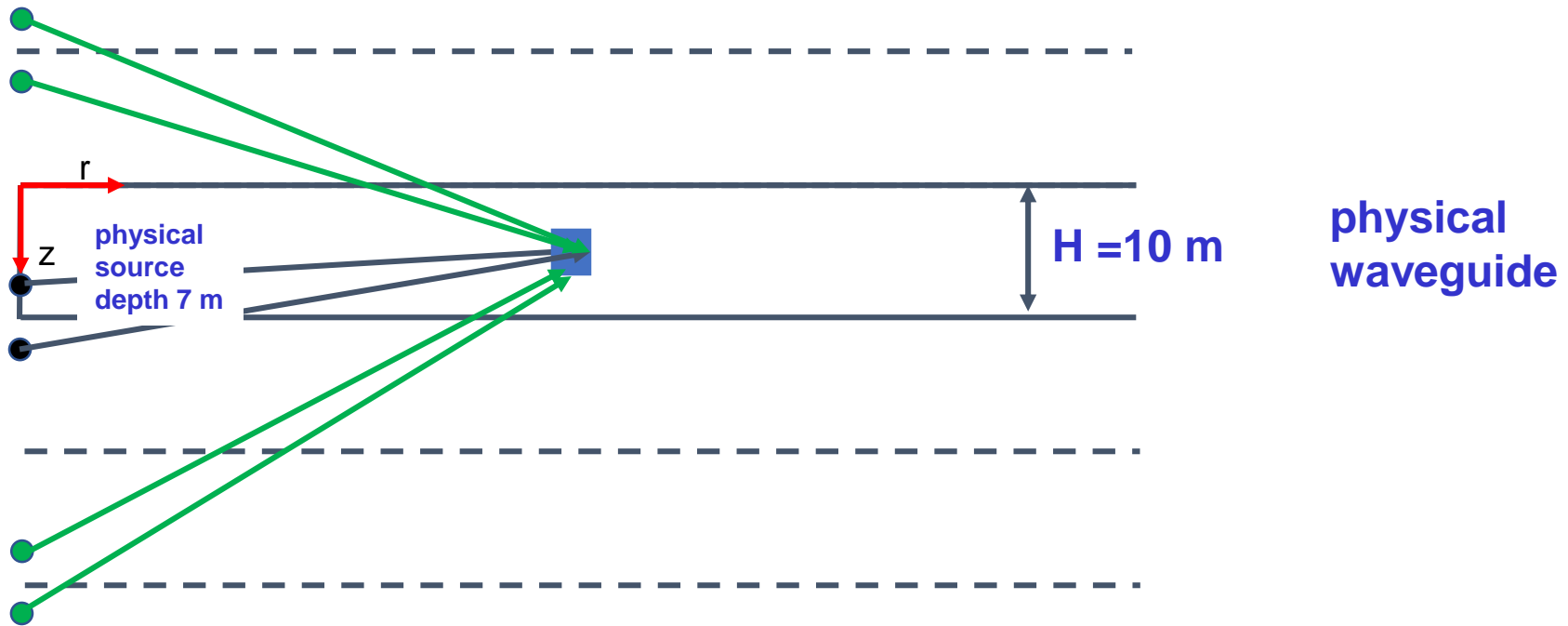


Positive image source below the boundary solves lower boundary condition.

But now upper boundary condition not satisfied

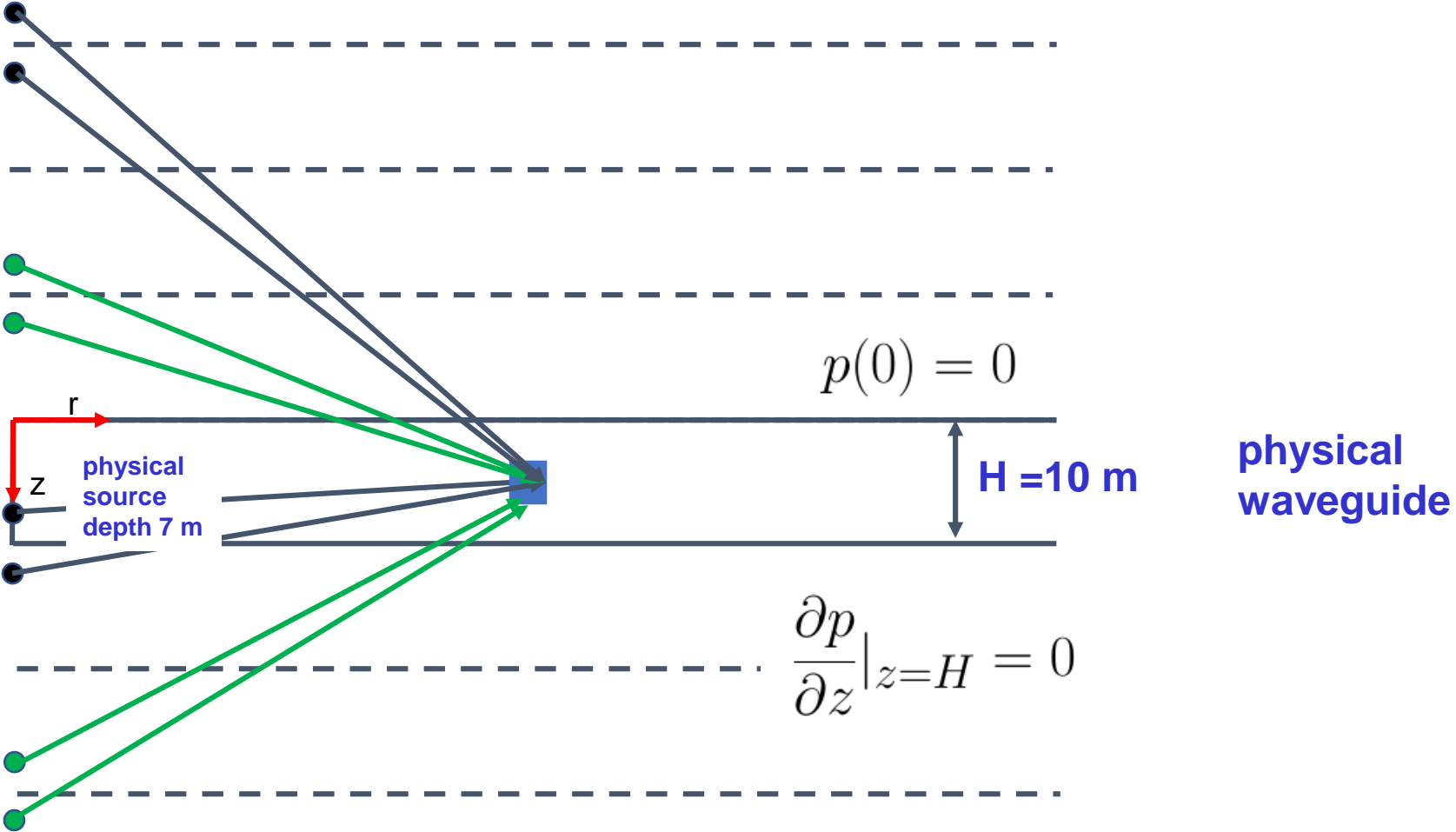
Two negative image sources now needed to solve upper boundary condition



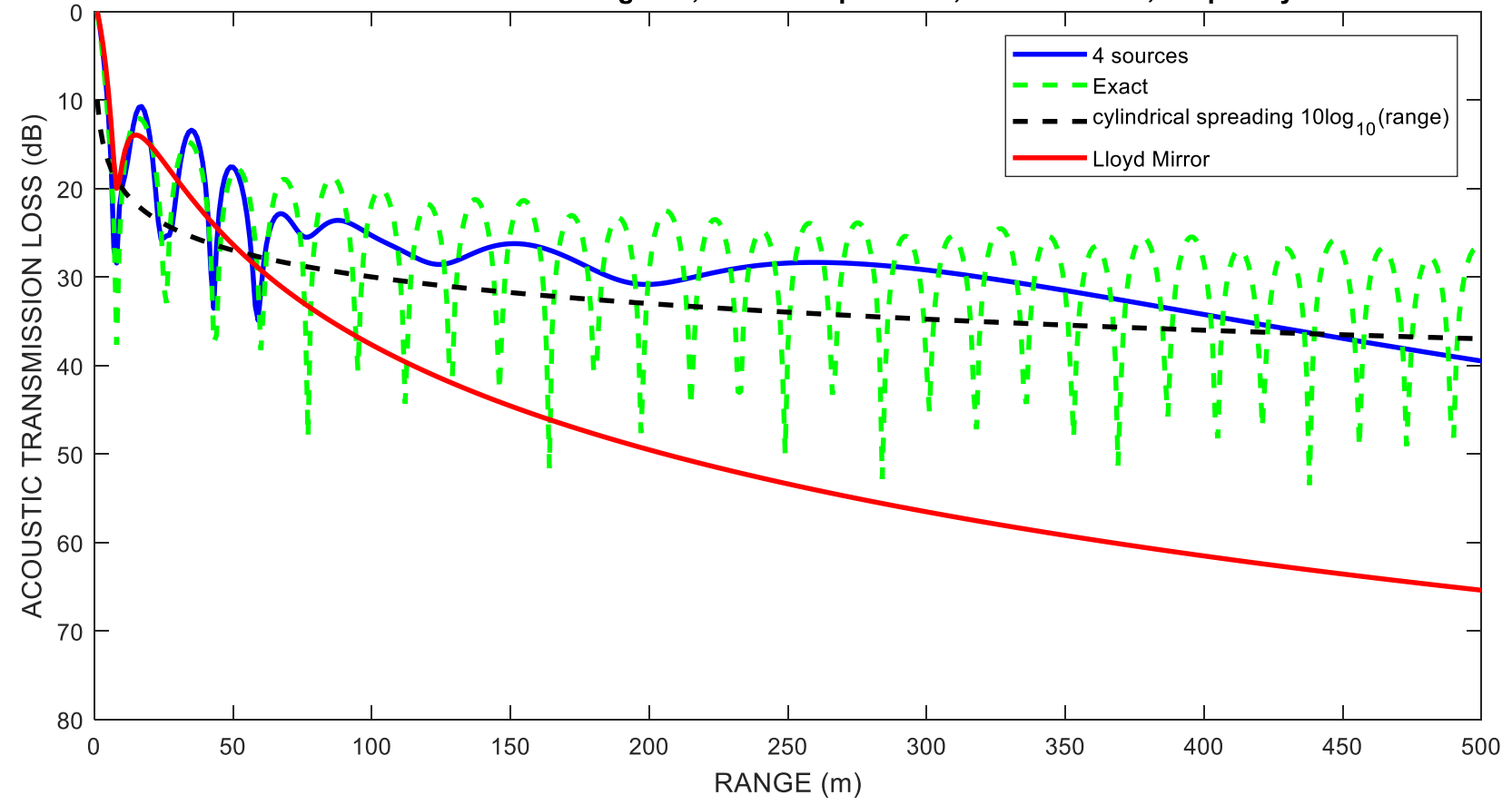


Now need two negative image sources here to solve lower boundary condition

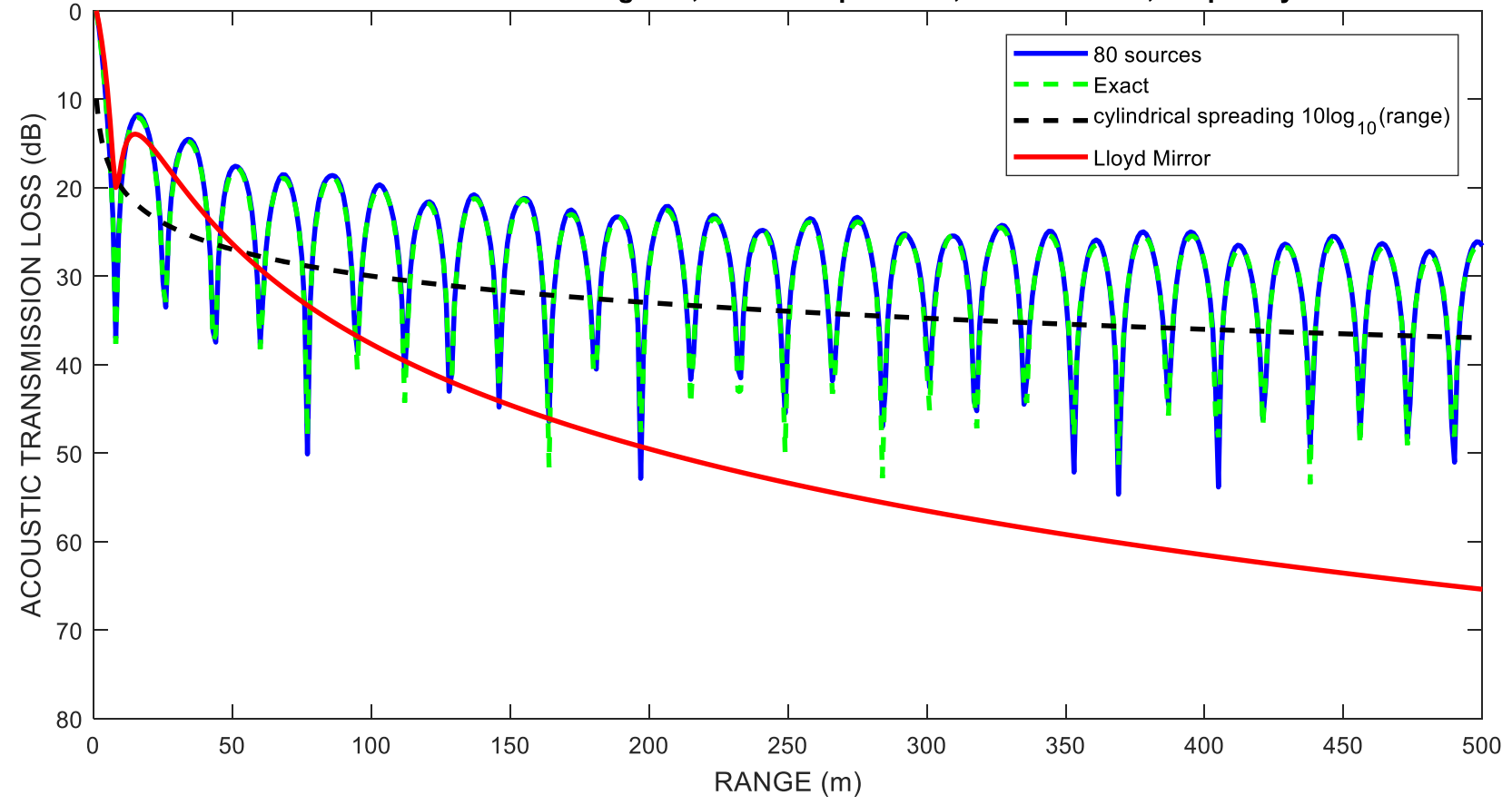
Two more positive image sources here to solve upper boundary condition.. and so on for infinite number of images!



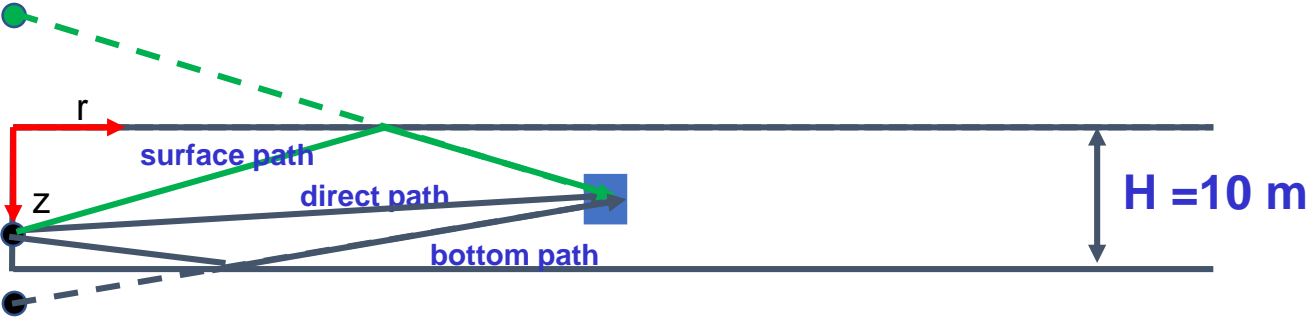
Transmission loss for 10-m waveguide, source depth =7 m, receiver = 5 m, frequency 240 Hz



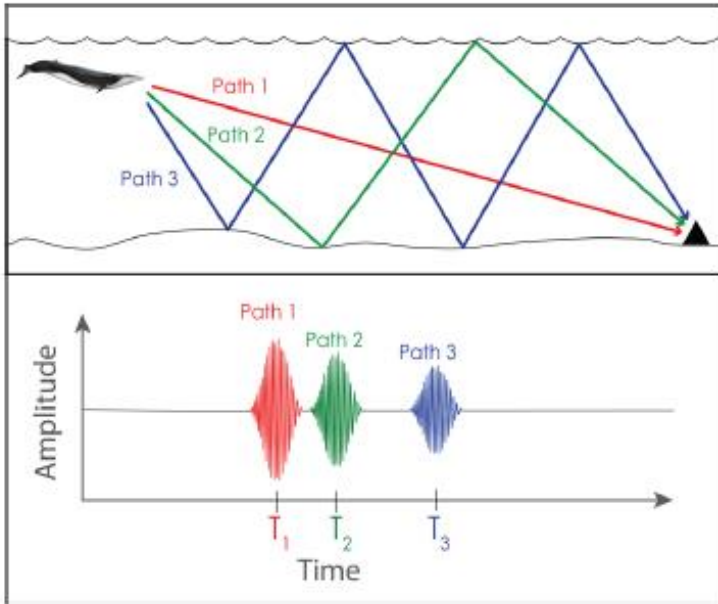
Transmission loss for 10-m waveguide, source depth =7 m, receiver = 5 m, frequency 240 Hz



Think of the image sources as additional paths from source to receiver. This is called multi-path propagation in waveguide



physical waveguide

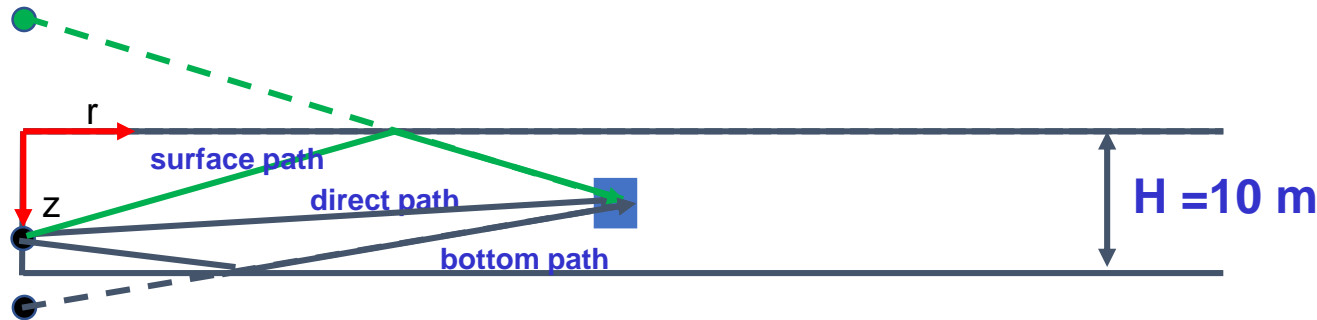


Here is how it occurs in an underwater waveguide

Figure reprinted from

**Estimating range to a vocalizing fin whale using the timing and amplitude of multipath arrivals**

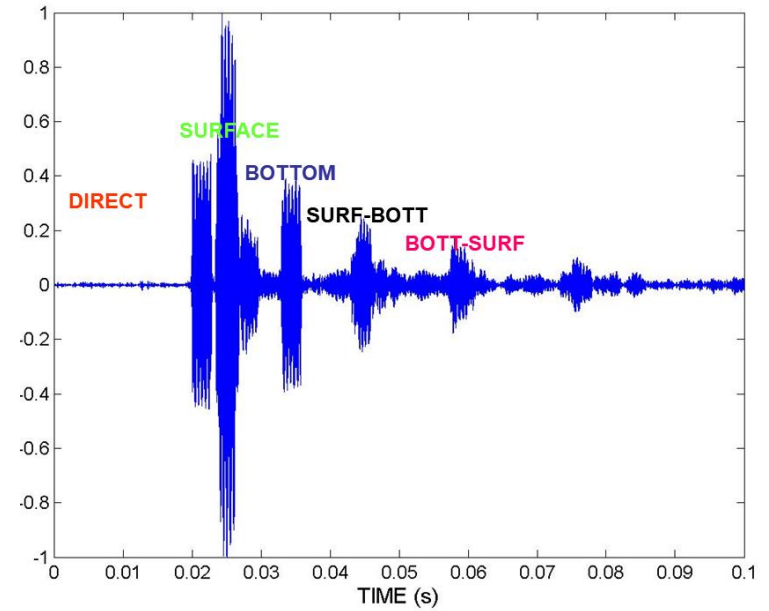
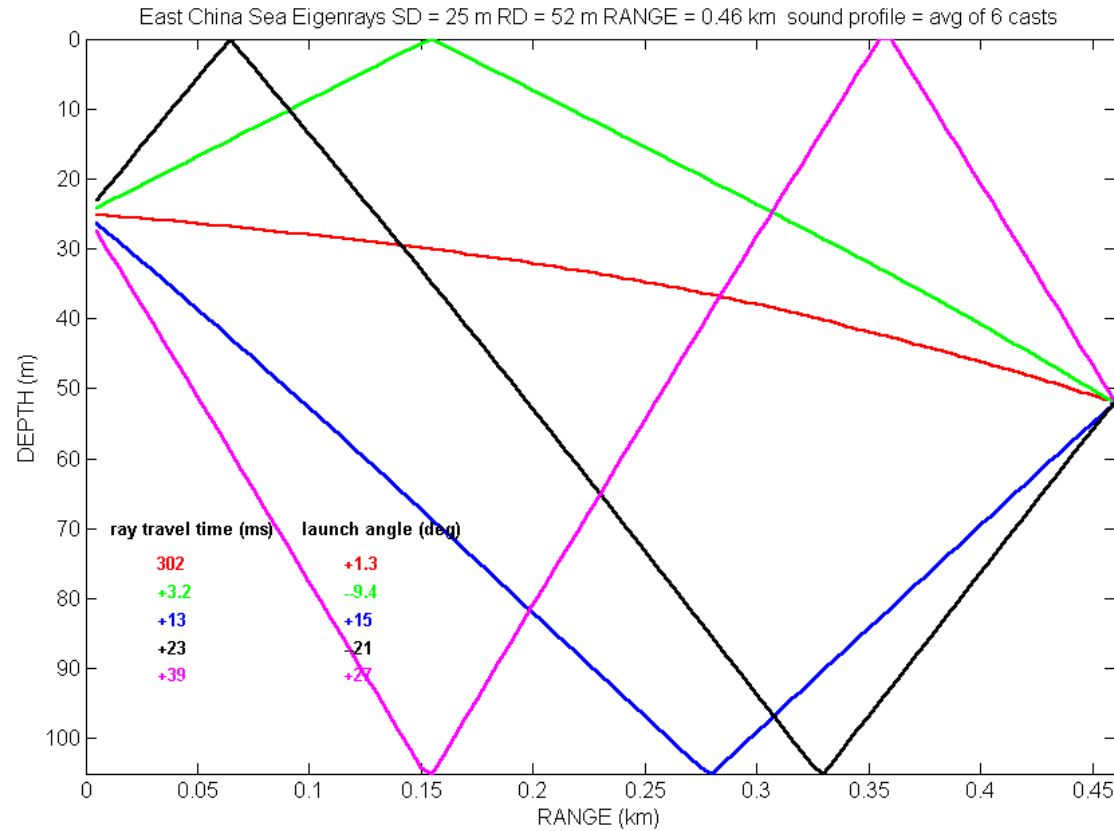
Michelle J. Weirathmueller,<sup>a)</sup> William S. D. Wilcock, and Rose S. Hilmo  
*School of Oceanography, University of Washington, Seattle, Washington 98195, USA*



**physical  
waveguide**

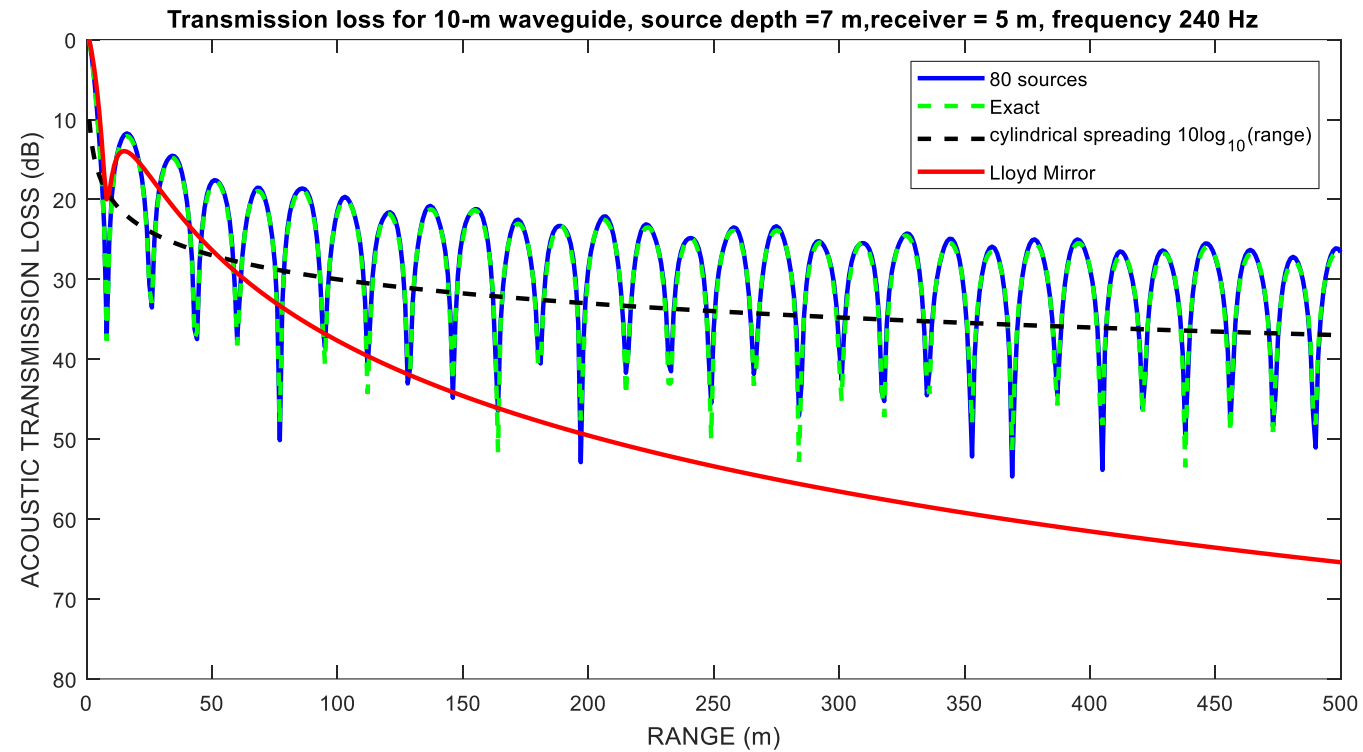
# Eigenrays (specific receiver identified)

Multipath propagation in the East China Sea, depth ~ 100 m



How do we get this kind of accuracy without using 100's images, and how can we address more realistic bottom boundary conditions?

Next: Method of Normal Modes



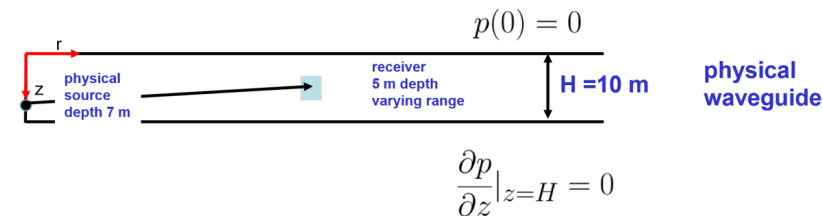
# ME525 Applied Acoustics Lecture 23, Winter 2022

## Method of Normal Modes

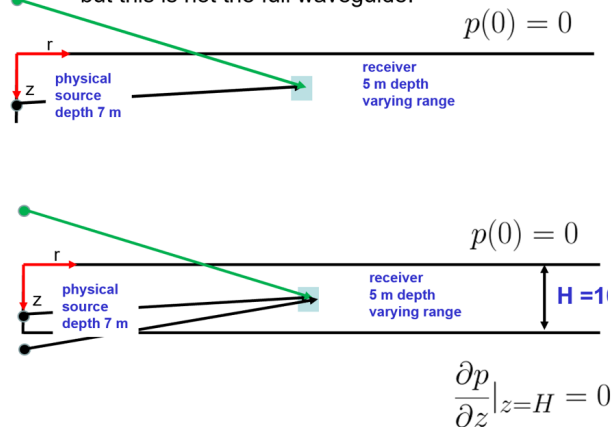
Peter H. Dahl, University of Washington

### About Normal Modes

Last time we saw how the method of images yields a "theoretical" exact solution to the problem of a point source within a waveguide, with upper boundary condition (at  $z = 0$ ) of  $p(0) = 0$ , and lower boundary condition (at  $z = H$ ) of  $\frac{\partial p}{\partial z}(H) = 0$ —provided enough images are used to reach a degree of convergence.



use negative image source to solve surface boundary condition (Lloyd Mirror problem). Already know this problem—but this is not the full waveguide.



Positive image source below the boundary solves lower boundary condition.

But now upper boundary condition not satisfied

Figure 1: An apparent problem with the method of images once two boundaries at  $z = 0, H$  introduced.

The negative image source above the  $z = 0$  boundary combines with true source within the waveguide to satisfy the boundary condition at  $z = 0$ , and the positive image below the  $z = H$  boundary combines with the true source to satisfy the boundary condition at  $z = H$ . But now, for example, the true source plus positive image require a second negative image source to satisfy

boundary condition at  $z = 0$ . The process of balancing out positive and negative image sources continues on and on to infinity or until some degree of convergence is reached.

This solution is from Frisk (Eq. 4.82, p. 83). It's relatively easy to code up—but you need to be careful to keep track of the expanding set of sources, whether they are negative or positive sign, and the ever changing magnitude of  $|\vec{r} - \vec{r}_i|$ . There is also some degree of likeness between rays and images, for example take the middle plot of Fig. 1; the direct ray from source to receiver is the black path and surface-reflected ray generated by the image is the surface-reflected path.

To reach convergence I needed about 80 images, although perhaps considerably fewer might suffice for an approximate solution. In contrast a simpler approach was achieved using the method of normal modes (Fig. 2). From this figure I can tell that about 2 or 3 modes were needed. What are these modes?

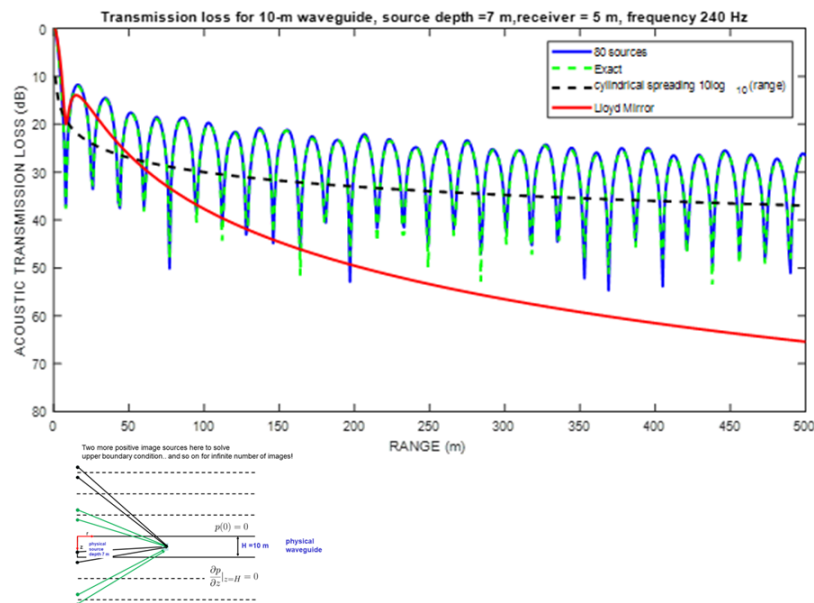


Figure 2: Comparison of image method (80 images) and method of normal modes requiring 2 modes.

Before turning our attention to underwater waveguides, Fig. 3 shows the pressure distribution within a tube for which in one case (left side) the frequency  $f$  is such that  $f < \frac{c}{1.7d}$  where  $d$  is tube diameter, and one axial mode is excited. This was alluded to in Lecture 20 for the discussion on the single expansion chamber Muffler problem. Increasing the frequency (right side) produces excitation of more modes within the tube the single, axial mode approximation used to study the Muffler no longer applies.

We now focus on the underwater waveguide and an excellent experiment to understand modes in this environment comes from the study by Frisk, Lynch and Rajan (1989). Figure 4 shows the experimental geometry to measure mode in Nantucket sound. There are two acoustic receivers (hydrophones) on a buoy at depth 7.1 m and 12.5 m. An acoustic source suspended from a research

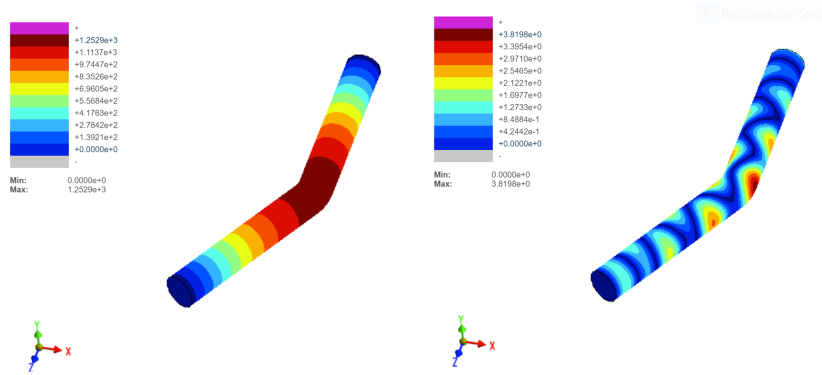


Figure 3: Left: pressure distribution within a bent tube frequency  $f$  is such that  $f < \frac{c}{1.7d}$  where  $d$  is tube diameter; thus only one axial mode shown. Right: pressure distribution frequency  $f > \frac{c}{1.7d}$  and several modes are excited.

vessel slowly moves away (opens in range) from these receivers, which are recording continuous wave (cw), or narrowband, sound at center frequency 140 Hz and 220 Hz. Thus, in terms of modeling of the receive sound the frequency content, and time dependence  $t$ . can be described with  $e^{-i\omega t}$  where  $\omega = 2\pi f$  and  $f$  is either 140 Hz or 220 Hz.

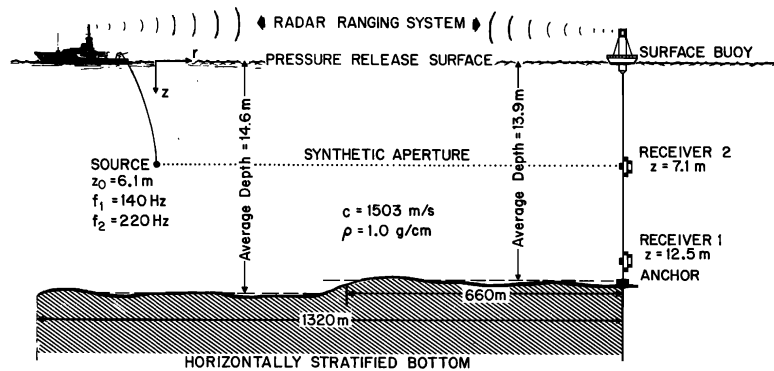


Figure 4: Geometry of experiment off Nantucket. Figure is Fig. 1 of Frisk, Lynch and Rajan (1989).

As the ship slowly opens in range from receivers which transmitting at these frequencies, modal interference patterns (Fig. 5) that depend on frequency and receiver depth, will be registered. I can tell right off that there about two modes in the interference pattern for 220 Hz shown in Fig. 5. Increasing the frequency well beyond 220 Hz will lead to a more complicated pattern owing to more than two modes, which decreasing the frequency substantially below 220 Hz will eventually yield just one mode. Lowering the frequency even further, say to about 100 Hz, then no modes are propagating: the *cutoff* frequency for this waveguide of depth about 15 m as been reached. This estimate (with notation and form recast slightly) originates from (1986)

$$f_n = \frac{c_w}{2H} \left[ \frac{n - 1/2}{\sqrt{1 - c_w^2/c_b^2}} \right] \quad (1)$$

where  $f_n$  is the cutoff frequency for the  $n^{\text{th}}$  mode,  $H$  is water depth, and  $c_w, c_b$  are water and seabed sound speeds, respectively. Thus my estimate of  $\sim 100$  Hz applies to the case of  $n = 1$

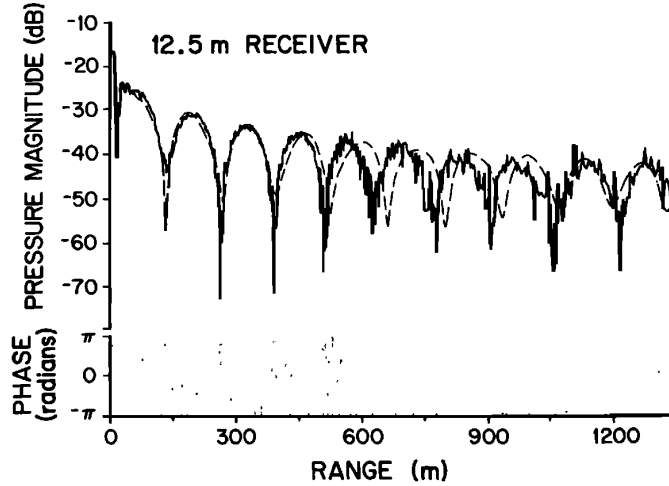


Figure 5: Transmission loss data for frequency 220 Hz, measured at depth 12.5 m versus range from source. Figure constitutes a portion of Fig. 3 of Frisk, Lynch and Rajan (1989). (The phase variation is not reproducible on line from this 1989 publication.)

The similarity between the simple model demonstration in Fig. 2 and the real data in Fig. 5 should be clear, both representing about two modes, and both showing an interference pattern with deep nulls, where the level of acoustic field drops precipitously then rises again. But let's address head on the obvious differences in notation between Figs. 2 and 5—and you need to get used to seeing such differences. In Fig. 2, I computed some kind of Green's function  $g(z, r; z_0)$ , as function of range  $r$ , receiver depth  $z$  and source depth  $z_0$ , e.g., for the image method  $g$  would have similarities to Eq.(1) of Lecture 10, but of course now many images are needed for the result in Fig. 2. My plot is  $-20 \log_{10} \frac{|g(z, r; z_0)|}{|g(z, r=1\text{m}; z_0)|}$ , so the value at  $r = 1$  m equals 0 dB, and for increasing ranges the field decays  $20 \log_{10}$  being increasingly negative, hence  $-20 \log_{10}$  yields a positive result. I call the result "Transmission Loss" or TL and plotting this way gives the intuitive result of increasing TL with increasing range.

The Frisk *et al.* results appear as "Pressure magnitude" as in  $-20 \log_{10} |p|$ , but also appear to be normalized in some manner, perhaps as  $-20 \log_{10} \frac{|p(12.5, r; 6.1)|}{|p(12.5, r=1\text{m}; 6.1)|}$ , where 12.5 and 6.1 represent the receiver and source depths, respectively. For example, in Fig. 5 the  $|p|$  at range 500 m relative to  $|p|$  at 1 m, appears to be about 30 to 40 dB less, which is not too different from my plot suggesting TL is in about this range (just as a very rough comparison as frequencies).

## The Method Normal Modes

The waveguide coordinate system (Fig. 6) is expressed in cylindrical coordinates  $(r, \theta, z)$ . There

is symmetry in the  $\theta$  direction, and the field is independent of  $\theta$ ; we need only to find the dependence in the  $r, z$  plane (white, dashed box in Fig. 2). The  $\theta$  independence also means the final solution applies to any rotation about the  $z$ -axis in Fig. 6. Thus the new problem involves the Laplacian operator in cylindrical coordinates without dependence on  $\theta$

$$\nabla^2 = \frac{1}{r} \frac{\partial}{\partial r} \left( r \frac{\partial}{\partial r} \right) + \frac{\partial^2}{\partial z^2}. \quad (2)$$

and look for new Green's function which satisfies the inhomogeneous Helmholtz equation for a point source at  $z = z_s$  and  $r = 0$

$$(\nabla^2 + k^2)g(r, z, z_s) = -2 \frac{\delta(r)}{r} \delta(z - z_s). \quad (3)$$

The delta function expression on the right is different from the one we encountered previously. Here it represents a point source at source located at  $z = z_s$  and  $r = 0$  in cylindrical coordinates (Frisk, 1994, Kinsler *et al.*, 1980).

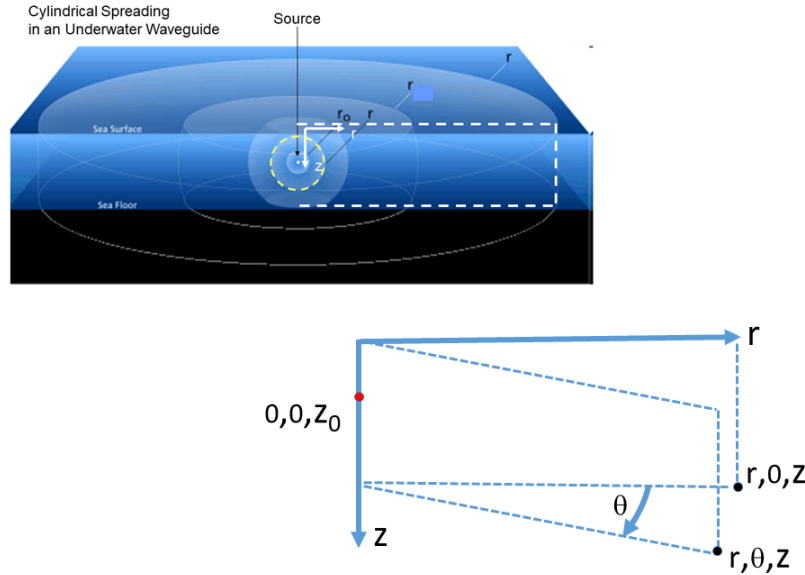


Figure 6: Cylindrical coordinate system for solving the wave equation in a waveguide. A source point (red) is located at depth  $z_0$  with  $r = 0$ , and two receiver points (black) located at  $r, \theta, z$  and  $r, 0, z$ . The analysis assumes no dependence in the  $\theta$  direction.

Equation (3) is separable, meaning separate solutions for range  $R_n(r)$  and depth  $U_n(z)$  are found and multiplied together for solution in  $r, z$ . In doing so, multiple solutions corresponding modes will be found, where for example,  $U_n(z)$  corresponds to the  $n^{\text{th}}$  mode. These are summed for the

final solution

$$g(r, z, z_s) = \sum_n R_n(r) U_n(z). \quad (4)$$

The key effort involves finding the solution for the depth or  $z$ -dependent part,  $U_n(z)$  which responsible for satisfying the boundary conditions at the  $z = 0, H$

$$\left(\frac{\partial^2}{\partial z^2} + \gamma_n^2\right)U_n = 0. \quad (5)$$

Equation (5) is a familiar 1D wave equation (Helmholtz equation) along the depth dimension  $z$ , although here the wavenumber  $k$  first seen in the Helmholtz equation, is replaced by its vertical component, where  $\gamma_n^2 = k^2 - k_{rn}^2$ . The vertical  $\gamma_n$  and radial or horizontal  $k_{rn}$  components of the wavenumber  $k$  vary according to mode number  $n$  but always satisfy  $\gamma_n^2 + k_{rn}^2 = k^2$ .

This relation is depicted in Fig. 7 and one can imagine, approximately, that a high order mode (large  $n$ ) corresponds to a ray with high grazing angle (steep ray) and low order mode (small  $n$ ) corresponds to ray with shallow angle. This subtle correspondence between modes and rays that is useful to keep in mind.

Underwater waveguide modes  $U_n(z)$  are not unlike modes of vibration of a guitar string, are functions that satisfy the boundary conditions in this case at the end points  $z = 0$  and  $z = H$ . As in the guitar string, there can be many modes satisfying the boundary conditions; for the guitar string the boundary condition is that the string is clamped at both ends and therefore does not vibrate at those points. For our waveguide case, the surface and bottom boundary conditions given above in the introduction are solved with  $U_n(z) = A_n \sin(\gamma_n z)$  where  $\gamma_n = \frac{(n-1/2)\pi}{H}$ , and  $A_n$  is a normalization constant (we discuss later). Note: the boundary condition was expressed in the form of pressure. The modes are not of dimension pressure *per se* but they are proportional pressure, or surrogate for pressure as in the Green's function. Thus if the  $U_n(z)$  satisfy the boundary conditions, so too does pressure.

The first three modes  $n = 1, 3$  (Fig. 8) for the underwater waveguide with same (idealized) boundary conditions used in Fig. 2, are shown frequency of 240 Hz and depth 10 m. One might call these mode functions, or eigenfunctions, and by inspection observe that these functions for modes 1,2,3 all equal 0 at  $z = 0$ , and their vertical derivative equals 0 at  $z = H$ . Another feature is correspondence between mode number  $n$  and the number of times the mode function equals 0 over the depth span, or *zero-crossings*. So the modes in this case appear to be some fraction of a sin wave, which in fact they are provided the sound speed within the water column does not change. This is a simplifying assumption that we maintain in this course, but the assumption is also often quite realistic.

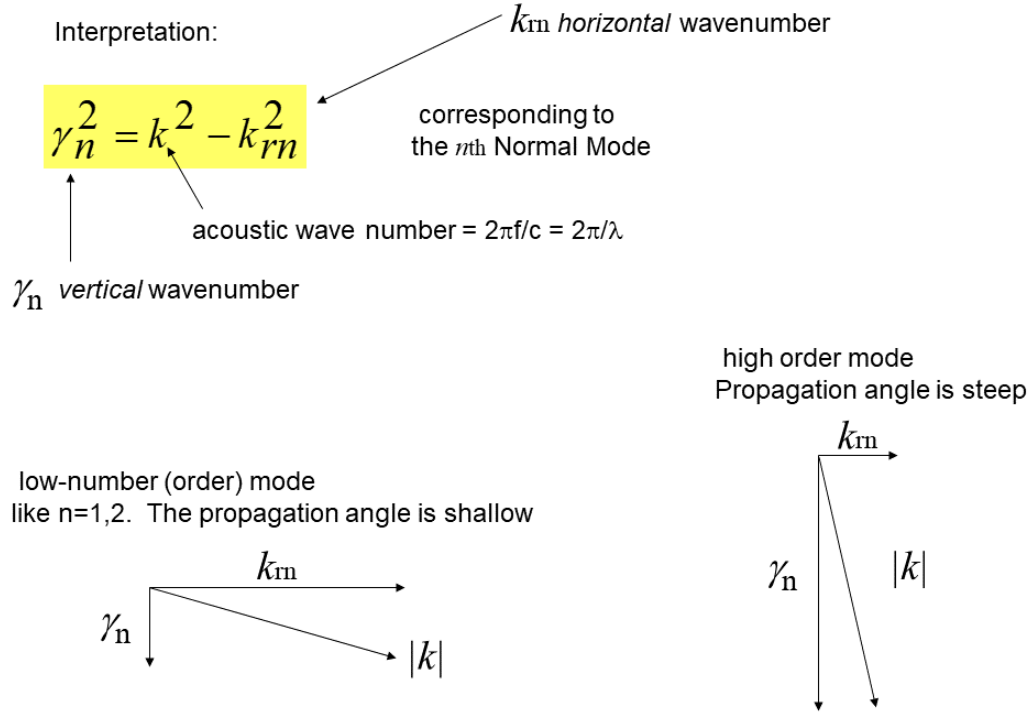


Figure 7: Interpretation of the wavenumber  $k$  in terms of its vertical  $\gamma_n$  and horizontal  $k_{rn}$  components.

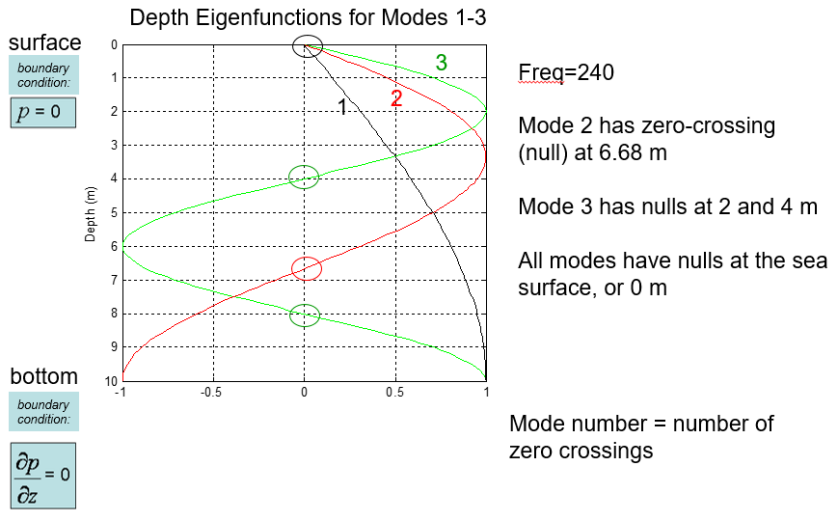


Figure 8: Eigenfunctions, or mode functions, for the first three modes for the case of frequency 240 Hz, depth 10 m. All modes have a zero-crossing at the surface, at  $z = 0$ , which constitutes the only zero-crossing for mode 1.

Looking ahead to the next lecture the final solution is

$$g(r, z, z_s) = \frac{2\pi i}{H} \sum_n \sin(\gamma_n z) \sin(\gamma_n z_s) H_0^1(k_{rn} r) \tag{6}$$

where  $H_0^1$  is the zeroth-order Hankel function of the first kind, and is a member of the cylindrical Bessel family. Note the dimension for the Green's function  $g(r, z, z_s)$  is  $L^{-1}$  (spherically spreading) just as with the free-space Green's function and method of images. However upon combining all these modes (or combining all those images in the method of images), we get a solution for pressure in the underwater waveguide that somewhat magically translates to pressure  $\sim 1/\sqrt{r}$  where  $r$  is range from source.

### References

- Frisk, G. V. *Ocean and Seabed Acoustics* (Prentice Hall, Englewood Cliffs, NJ, 1994)
- Frisk, G. V., J. Lynch and S. Rajan, "Determination of the compressional wave speed profiles using modal inverse techniques in a range-dependent environment in Nantucket sound," *J. Acoust. Soc. Am.* 86, Nov. 1989.
- L. E. Kinsler, A. R. Frey, A. B. Coppens, and J. V. Sanders, *Fundamentals of Acoustics*, (John Wiley & Sons, New York, 1980)

# ME525 Applied Acoustics Lecture 24, Winter 2022

## Method of Normal Modes

Peter H. Dahl, University of Washington

### Details on the Green's function $g$ derived from the Method of Modes

The goal is to find a Green's function,  $g$  that satisfies the inhomogeneous Helmholtz equation for a point source at  $z = z_s$  and  $r = 0$

$$(\nabla^2 + k^2)g(r, z, z_s) = -2\frac{\delta(r)}{r}\delta(z - z_s). \quad (1)$$

The structure of the delta function in Eq. (1) looks different from that of say, Eq.(13) of Lecture 8, because the Helmholtz equation has been recast in this cylindrical coordinate system (Fig. 1). The equation could have been solved by repeated use of the method of images.

However as noted last time this equation is separable into its  $r$ -dependent and  $z$ -dependent parts, and now we find  $g(r, z, z_s)$  in terms of the sum of mode functions  $U_n(z)$  multiplied by the corresponding  $R_n(r)$ , as in

$$g(r, z, z_s) = \sum_n R_n(r)U_n(z). \quad (2)$$

This yields a considerably useful and flexible solution approach.

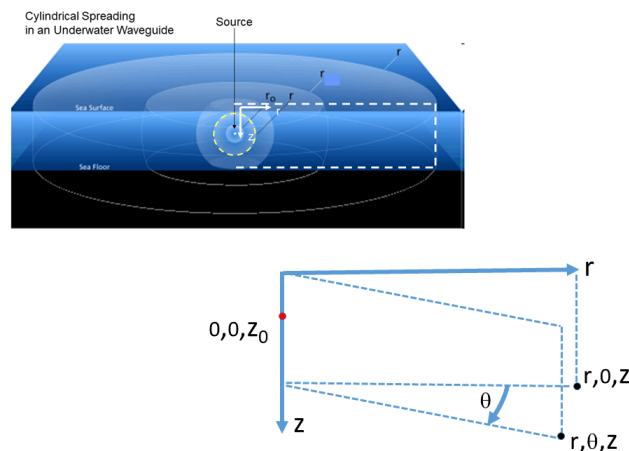


Figure 1: Cylindrical coordinate system for solving the wave equation in an underwater waveguide. A source point (red) is located at depth  $z_0$  with  $r = 0$ , and two receiver points (black) located at  $r, \theta, z$  and  $r, 0, z$ . The analysis assumes no dependence in the  $\theta$  direction.

The radial part  $R_n(r)$  has only one boundary condition known as the Sommerfeld radiation condition (e.g., see Frisk, 1994), for which one interpretation is that at large range  $r$  the field takes on

plane-wave behavior, with the wave impedance becoming more like the characteristic impedance. For example, the radial dependence is not unlike ripples on water surface produced by point disturbance (as in dropping a rock), with the waves becoming more planar like the greater the range  $r$  from the source point on the surface.

It is with the vertical part where the surface and bottom boundary conditions are addressed, and the key effort reduces to finding the solution for the depth or  $z$ -dependent part,  $U_n(z)$  to

$$\left(\frac{\partial^2}{\partial z^2} + \gamma_n^2\right)U_n = 0. \quad (3)$$

along with satisfying boundary conditions at the  $z = 0, H$ . The wavenumber  $k$  in Eq.(1) is broken up in vertical  $\gamma_n$  and horizontal  $k_{rn}$  components that vary according to mode number  $n$  and always satisfy  $\gamma_n^2 + k_{rn}^2 = k^2$ .

Equation (3) should be familiar problems of vibration and simple oscillations;  $U_n(z)$  takes the form  $\sin(\gamma_n z)$ . We find  $\gamma_n$  via the eigenvalue equation

$$\gamma_n = \frac{(n - 1/2)\pi}{H}, \quad (4)$$

such that boundary conditions are satisfied. Try it:  $U_n = \sin(\gamma_n z)$  thus  $U_n|_{z=0} = 0$  and  $\frac{\partial U_n}{\partial z}|_{z=H} = 0$  for  $n = 1, 2, 3, \dots$ . Looking ahead, Eq.(4) represents the most elementary of eigenvalue equations that is solvable exactly without numerical means. The situation is made more complicated when a real seabed with sound speed  $c_b$  and density  $\rho_b$  are added to the picture.

### Orthonormality of mode functions $U_n$

An important property of  $U_n$  is that this function be orthonormal such that integral over depth is

$$\int_0^H U_n U_m dz = \delta_{nm} \quad (5)$$

where  $\delta_{nm}$  is the Kronecker delta symbol which equals 1 for  $m = n$  and 0 for  $m \neq n$ . For certain this integral equals 0 for  $m \neq n$ , but to equal 1  $m = n$  a normalization constant  $A_n$  is needed such that  $U_n(z) = A_n \sin(\gamma_n z)$ , with normalization requiring that  $A_n$  equal to  $\sqrt{\frac{2}{H}}$ . For this case the normalization constant  $A_n$  is the same for all modes but in general there will be a dependence on mode number  $n$ .

### Details on the radial dependence $R_n(r)$

The next step represents a traditional approach for solving partial differential equations that are

separable. First insert Eq.(2) as candidate solution to Eq. (1) yielding

$$\sum_n \nabla^2 R_n(r) U_n(z) + k^2 R_n(r) U_n(z) = -2 \frac{\delta(r)}{r} \delta(z - z_0) \quad (6)$$

Now break up the  $\nabla^2$  operator into  $r$  and  $z$  dependencies. This leads to the following upon exploiting Eq. (3),

$$\sum_n U_n \frac{1}{r} \frac{\partial}{\partial r} \left( r \frac{\partial R_n}{\partial r} \right) + R_n k_{rn}^2 U_n = -2 \frac{\delta(r)}{r} \delta(z - z_s). \quad (7)$$

Note: there was a wavenumber  $k$  in Eq.(6), now we got a  $k_{rn}$  in Eq.(7), what happened? We devised a separation constant to split in the partial differential equation into  $r$  and  $z$  dependencies, where  $k^2 = k_{rn}^2 + \gamma_n^2$ . Adapt this language for consistency with Fig. 7 of Lecture 23:  $k_{rn}^2$  is the *horizontal wavenumber* for the  $n^{\text{th}}$  mode;  $\gamma_n^2$  is the *vertical wavenumber* for the  $n^{\text{th}}$  mode.

Now multiply both sides of Eq.(7) by  $U_m$  and integrate over depth  $z$  from 0 to  $H$ , and invoke the *orthonormal property* along with the *sifting property* of the delta function, to yield

$$\frac{1}{r} \frac{\partial}{\partial r} \left( r \frac{\partial R_m}{\partial r} \right) + R_m k_{rm}^2 = -2 \frac{\delta(r)}{r} U_m(z_s) \quad (8)$$

The above represents a purely radial form of the Helmholtz equation with point source at origin  $r = 0$  (e.g. somewhat akin to ripples on the surface of a pond, the pond being of infinite extent) but multiplied by the constant  $U_m(z_s)$  since the source depth  $z_s$  is a fixed value. (The change from  $k_{rn}$  to  $k_{rm}$  being of no significance, merely a result of our choosing to go with  $U_m$ .)

The solution is well-known and solved by functions of the cylindrical Bessel family, in this case the zeroth-order Hankel function of the first kind which we denote as  $H_0^1$ . The solution for index  $n$  is

$$R_n(r) = i\pi H_0^1(k_{rn}r) U_n(z_s) \quad (9)$$

where  $U_n(z_s)$  provides the dependency on source depth needed for the Green's function.

Type "help besselh" in Matlab to obtain more information about  $H_0^1$ . In Matlab evaluate  $H_0^1(k_{rn}r)$  as `besselh(0, 1, krn * r)`, where  $r$  is vector of ranges and  $k_{rn}$  is horizontal wavenumber for the  $n^{\text{th}}$  mode. A useful approximation for  $H_0^1(k_{rn}r)$  valid for  $k_{rn}r \gg 1$  is

$$H_0^1(k_{rn}r) \approx \sqrt{\frac{2}{\pi}} e^{-i\pi/4} \frac{e^{ik_{rn}r}}{\sqrt{k_{rn}r}} \quad (10)$$

The final solution is thus

$$g(r, z, z_s) = \frac{2\pi i}{H} \sum_n \sin(\gamma_n z) \sin(\gamma_n z_s) H_0^1(k_{rn}r) \quad (11)$$

Notice that the basic dimension for the Green's function  $g(r, z, z_s)$  is  $L^{-1}$ , owing to the  $1/H$  dependence out front, but the behavior for far ranges is  $\sim 1/\sqrt{r}$  which can be more clearly seen in the asymptotic expression of Eq. (10).

### The number of modes and cut-off frequency

So, given the important behavior apparent in Eq. (10),  $\frac{e^{ik_{rn}r}}{\sqrt{k_{rn}r}}$ , it should be clear that if  $k_{rn}$  becomes imaginary to any significant degree, that mode will not go very far. For example, take the waveguide examined previously (Fig. 2) with frequency 240 Hz,  $H = 10$  and water sound speed 1450 m/s. Run through Eq.(4) starting from  $n = 1$  and compute the corresponding  $k_{rn}$ , get:

Table 1: Modes for waveguide of  $H = 10$  m, frequency 240 Hz,  $c_w = 1450$  m/s, and  $k = 1.04 \text{ m}^{-1}$

Mode number	$\gamma_n$	$k_{rn}$	Will this mode propagate?
1	0.15713	1.0280	yes
2	0.4712	0.9271	yes
3	0.7854	0.6817	yes
4	1.0996	$i$ 0.357	nope!

Obviously the vertical wavenumber continues to grow with increasing mode number, and once it exceeds the wavenumber in the water column  $k$  then,  $k_{rn}$  becomes imaginary. Note: which imaginary do we take from the square root, the positive or negative? In ME 525 with  $e^{-i\omega t}$  dependence, you *must* take the positive square root to make Eq.(10) work properly. So, clearly the number of modes in this example is three, or it is said there are three *trapped* modes in this waveguide.

Now Fig. 2 looks to me that there are about two trapped modes, given the regular interference pattern, rather than three that we infer from Table 1. Check out Fig. 8 from Lecture 23 where I plot the  $U_n$  for these three modes. It looks like the source depth I chose—7 m—was very close to the zero crossing of mode 2, so this mode was weakly excited.

Take the case for depth  $H$  equal to 100 m (Fig. 3), where Eq. (10) now gives exactly 33 trapped modes before an imaginary  $k_{rn}$  emerges. Interestingly we can also reasonably approximate the solution with far fewer image sources, e.g., about 8 image sources (and even the simple Lloyd mirror solution consisting of just two image sources provides reasonable approximation up to ranges of about 50 m). Given we were able to liken image sources to the concept of an acoustic ray, these two examples illustrate an interesting trade off: when the acoustic field in the waveguide requires many modes to fully describe it, then typically it can be described with much fewer rays, and vice versa. It will no doubt pay in your research to keep this trade off in mind.

The number of modes in a waveguide of depth  $H$  depends on the sound frequency, or more precisely the sound wavelength  $\lambda$ , with a simple and useful rule of thumb for this number being

$$n_{\text{modes}} \approx 2H/\lambda \quad (12)$$

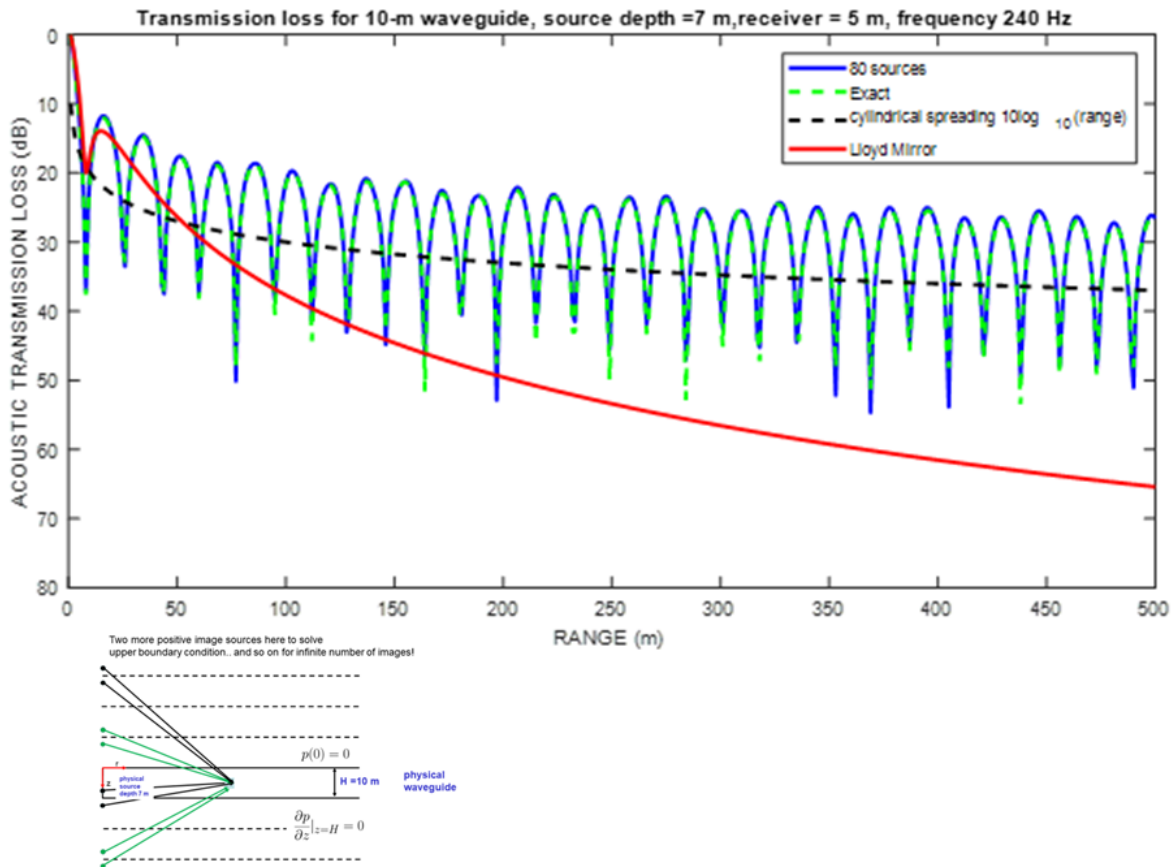


Figure 2: Upper: comparison of 80 image-source result with the method of normal modes. Lower: Layout for method of images based on sources of the form  $e^{ikR}/R$  where  $R$  depends on image location. Depth  $H = 10$  m

For this example of  $H = 10$  m,  $n_{modes}$  is 3.2, for  $H = 100$  m, there 10 times the number of modes.

Keep in mind Eq.(12) is the simplest of rules, which will need to be modified for more realistic boundary conditions at the seabed that involve finite sound speed and density for sediment, for example, refer to Fig. 1 of Lecture 18. We can compute the corresponding discrete horizontal angle call it  $\theta_n$  for each of the 33 trapped modes for the 100-m case (Fig. 4), where  $k_{rn} = \cos \theta_n k$ . These angle get quite steep for the high mode numbers, getting to about  $80^\circ$ . But, in the more realistic case  $\theta_n$  must be  $\leq \theta_c$ .

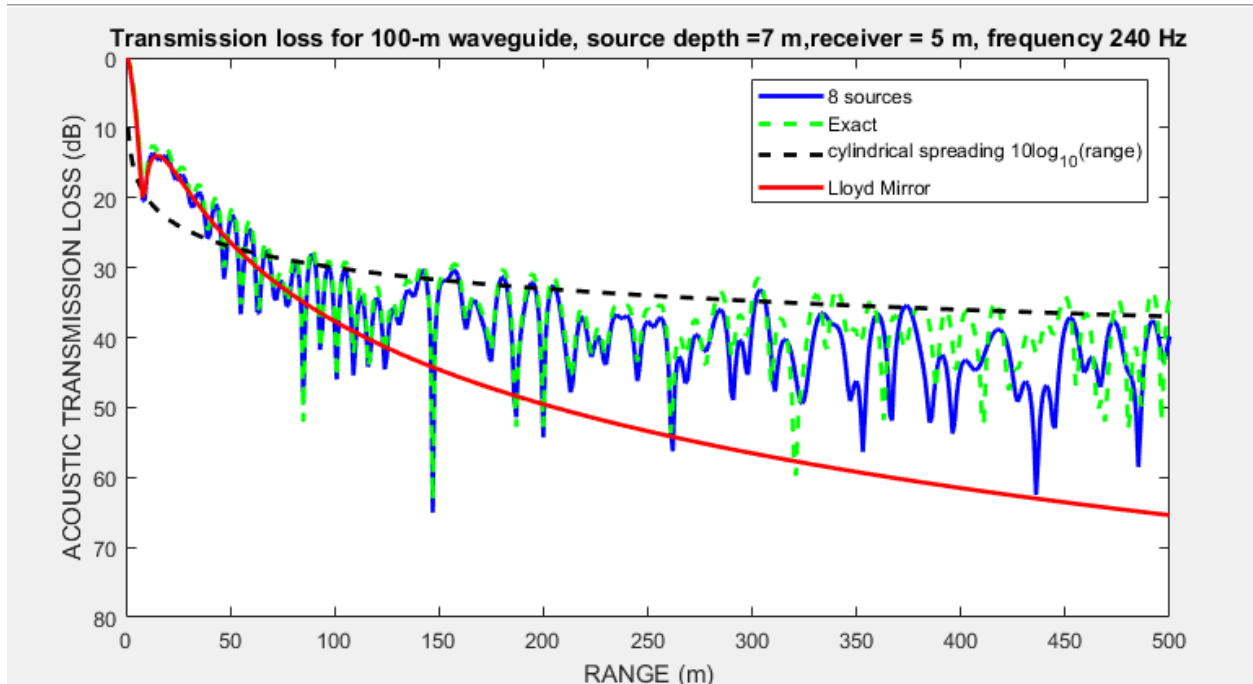


Figure 3: Acoustic transmission loss for waveguide with same boundary conditions, source frequency, and source/receiver depth as in Fig. 2, but with depth  $H = 100$  m.

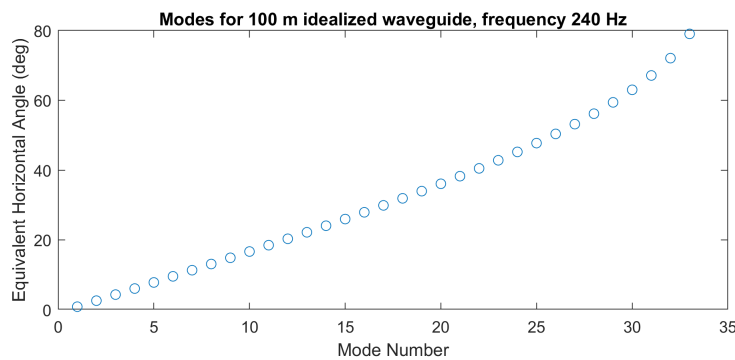


Figure 4: The discrete set of horizontal mode angles for the 33 trapped modes for the waveguide in Fig. 3, but with depth  $H = 100$  m.

## References

Frisk, G. V. *Ocean and Seabed Acoustics* (Prentice Hall, Englewood Cliffs, NJ, 1994)

# ME525 Applied Acoustics Lecture 25, Winter 2022

## Normal modes in more realistic waveguides

Peter H. Dahl, University of Washington

We continue with the discussion started at the end of Lecture 24, where the corresponding discrete horizontal angle, call it  $\theta_n$ , for each of  $n$ -trapped modes was computed, such that  $k_{rn} = \cos \theta_n k$ . It is thus useful to view each mode as having a discrete propagation angle, or a "specific preferred direction of propagation" for that mode (Frisk, 1994). Evidently the  $\cos$  of this angle relative to horizontal equals  $k_{rn}/k$ .

The sequence of discrete angles continues to increase starting from mode-1 (see Fig. 4 of Lecture 24) until no more propagating modes are found—the point at which  $k_{rn}$  becomes imaginary. Placement of such an imaginary  $k_{rn}$  into the argument of  $H_0^1(k_{rn}r)$  produces rapid, exponential decay as a function range  $r$ —easier to see in the asymptotic expression  $H_0^1$ . Such modes are known as evanescent modes.

Now, the simple model for boundary conditions at  $z = 0, H$  (Fig. 1, upper) is useful because it exhibits properties of the *discrete angular spectrum* associated with trapped modes. However this rigid boundary condition on the seabed does not permit a critical angle—the assumption being that the sound speed in the seabed is infinite, and the boundary represents an *infinite impedance boundary*. With presence of a critical angle, there is a more interesting transition between trapped modes and those with higher mode numbers. We make the problem considerably more realistic (Fig. 1, lower) without too much more effort by including the plane wave reflection coefficient  $R$  representing reflection at the boundary between an upper (water) medium with sound speed  $c_1$  and a lower (sediment) medium with sound speed  $c_2$ . From our earlier study of  $R$  we found that a critical angle  $\theta_c$  is defined at  $\cos \theta_c = c_1/c_2$ .

The critical angle provides the demarcation (Fig. 2) between discrete angular spectrum (trapped modes) with propagation angles  $< \theta_c$ , and the continuous angular spectrum with propagation angles  $> \theta_c$ . The discrete set of preferred propagation angles (blue rays) is within the yellow cone defined by the critical angle, outside of which is the continuous set of propagation angles (red rays) that can exist at a continuous range of angles all greater than  $\theta_c$ . Rays corresponding to the continuous set exist only close to the source (within about one or two water depths) because their contribution is quickly attenuated due to energy loss from propagation into the seabed. An approximate range after which the contribution is primarily from the discrete, trapped modes is  $R_o = \frac{H}{2 \tan \theta_c}$

### Modes in a realistic waveguide

With inclusion of realistic sound speed and density in the seabed we have an *finite impedance*

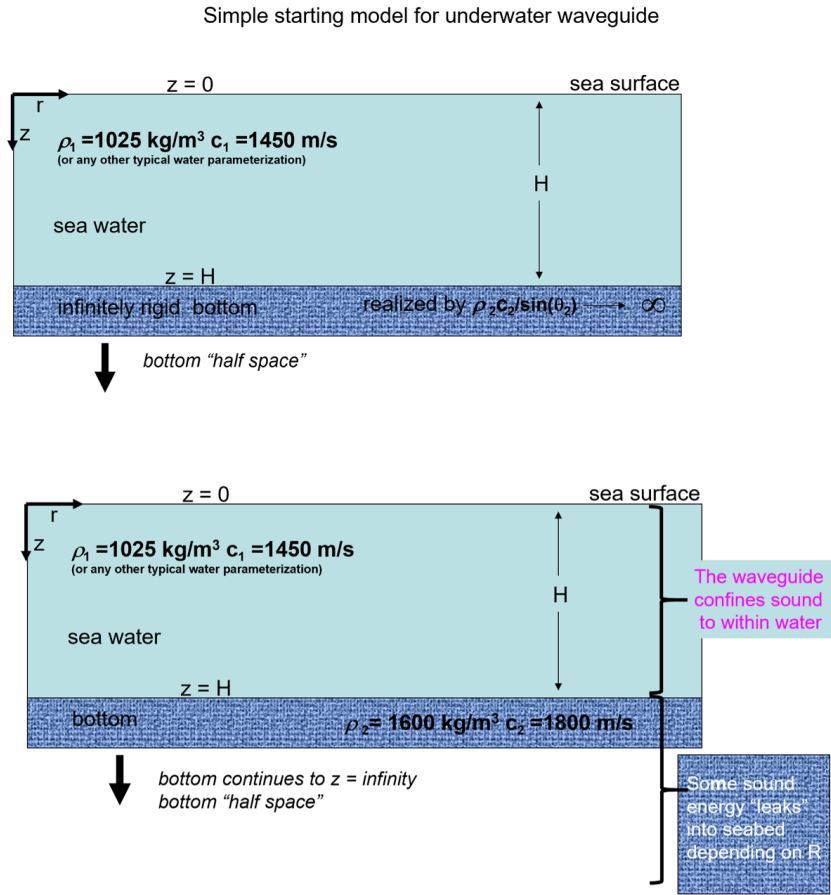


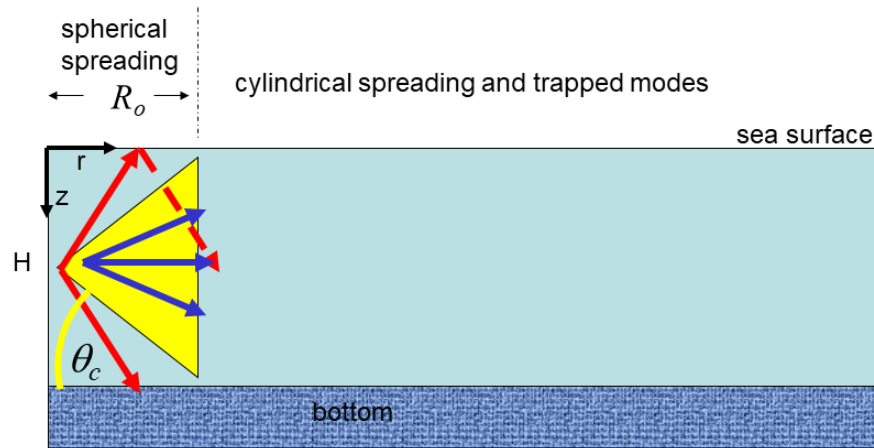
Figure 1: Upper: Idealized waveguide we have been studying with boundary conditions at  $z = 0, H$ , and solution given by Eq.(2). Lower: more realistic waveguide for which the plane reflection coefficient  $R$  describes the boundary condition at  $z = H$ .

boundary, as described by  $R$ . The new equation for solving for  $\gamma_n$  is

$$1 + Re^{2i\gamma_n H} = 0 \quad (1)$$

where remember that  $R$  is also a function  $\gamma_n$ . As a quick check, put  $R = 1$  corresponding to the infinite impedance boundary and recover the original specification for  $\gamma_n = \frac{(n-1/2)\pi}{H}$ . However, Eq.(3) is a transcendental equation that does not have closed-form solution. Instead numerical approaches, such as Newton Raphson, can be used to find the zeros of Eq.(3) as function of  $\gamma_n$ .

Without any numerical effort one can still get a quick visualization on where the modes are located by plotting  $|1 + Re^{2i\gamma_n H}|$  over a fine angular resolution (Fig. 3). Although this is not a recommended approach to finding the zeros of an equation one can immediately see where modes are located. In this example, water sound speed  $c_1 = 1525 \text{ m/s}$ , sediment sound speed  $c_2 = 1700 \text{ m/s}$ , water density  $\rho_1 = 1024 \text{ kg/m}^3$  and seabed density  $\rho_1 = 1800 \text{ kg/m}^3$ , with quantities sufficient to specify the plane wave reflection coefficient  $R$ . To identify specific modes we require a water



$$R_o \approx \frac{H}{2 \tan \theta_c}$$

$\theta_c$  The critical angle from analysis of the plane wave reflection coefficient  $R(\theta)$

Figure 2: Idealization depicting the discrete set of preferred propagation angles (blue rays) within the yellow cone as defined by the critical angle, and the continuous set of propagation angles (red rays) that can exist *angle* angles greater than  $\theta_c$ .

depth  $H = 50$  m, and frequency 200 Hz. The reflection coefficient (remaining fully complex) is computed over a fine grid of grazing angles  $\theta$  (Fig. 3 upper). For every such  $\theta$ , a  $\gamma = k_1 \sin \theta$  is identified, i.e., a continuous range of  $\gamma$  as distinct from a discrete set, such as  $\gamma_n$ . A plot of  $|1 + Re^{2i\gamma_n H}|$  (Fig. 3 lower) shows a set of minima, representing the discrete set of propagation angles for this waveguide. These angles (shown by the circles) are:  $3.9920^\circ$ ,  $8.0270^\circ$ ,  $12.1400^\circ$ ,  $16.3500^\circ$ ,  $20.668^\circ$ , and  $25.0530^\circ$ , values that are likely as close as one can get with a numerical approach. Note that the critical angle,  $26.22^\circ$  is greater than largest angle in the discrete set and effectively bounds these angles.

To summarize, the discrete angles – “preferred propagation angles” – of the trapped modes all must be less than critical angle. The modes are trapped, meaning they will travel far, given that the corresponding horizontal wavenumber for such a modes  $k_{rn}$  will be primarily real-valued, and not be purely, or even largely, imaginary, which leads severe exponential decay with increasing range. To be complete, there can be small imaginary component in  $k_{rn}$  to account for attenuation effects – but this is not the same as the mode being evanescent. Eventually solutions to Eq.(1) are not be found that can be considered as “trapped” modes– we run up against the critical angle  $\theta_c$ . In fact more solutions can be found, but belong to the realm of the continuous spectrum of angles, where

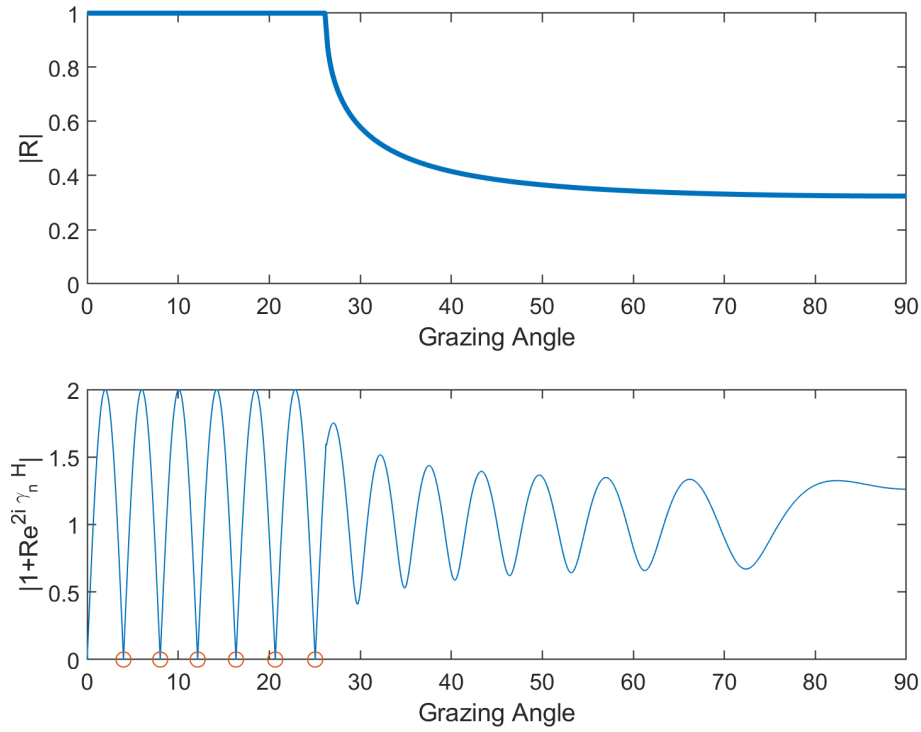


Figure 3: Upper: magnitude of the reflection coefficient  $|R|$ . Lower:  $L |1 + \text{Re}^{2i\gamma_n H}|$  over a fine angular resolution. The six minima to the left of the critical angle at  $26.22^\circ$  are trapped modes (not counting the first minimum), and are identified by circles.

the steep propagation angles lead to penetration into the seabed and significant energy loss with increasing range.

Here is very handy formula for the number of trapped modes in realistic underwater waveguide

$$\text{Number trapped modes} = \text{floor}\left(\frac{k_1 H}{\pi} \sin \theta_c + \frac{1}{2}\right) \quad (2)$$

which, upon applying the waveguide parameters discussed in Fig. 3, predicts the 6 modes.

### The field in a realistic waveguide

Let's be reminded of the solution studied thus far for the Green's function applied to a waveguide depth of  $H$ , with boundary conditions  $g|_{z=0} = 0$  and  $\frac{\partial g}{\partial z}|_{z=H} = 0$ , infinite impedance case for the seabed, which is

$$g(r, z, z_s) = \frac{2\pi i}{H} \sum_n \sin(\gamma_n z) \sin(\gamma_n z_s) H_0^1(k_{rn} r) \quad (3)$$

How is this solution changed with introduction of a more realistic, finite impedance seabed? Basically in two ways, one clearly involves a new set of discrete mode wavenumbers, be it the

vertical  $\gamma_n$  or the equivalent horizontal  $k_{rn}$ , the other being the mode normalization constant that goes from a constant  $A_n = \sqrt{\frac{2}{H}}$  to (Frisk, Eq. (5.144))

$$A_n = \sqrt{2} \left[ \frac{1}{\rho_1} \left( H - \frac{\sin 2\gamma_n H}{2\gamma_n} \right) + \frac{1}{\rho_2} \frac{\sin^2 \gamma_n H}{\gamma_{2n}} \right]^{-1/2}. \quad (4)$$

The revised Green's function becomes

$$g(r, z, z_s) = \frac{\pi i}{\rho_1} \sum_n A_n^2 \sin(\gamma_n z) \sin(\gamma_n z_s) H_0^1(k_{rn} r). \quad (5)$$

Continuing with the example discussed in Fig. 3, and with knowledge that there are more superior ways to find the modes, e.g., Zang and Tindle (1993), let us nevertheless use the six discrete angles found,  $\theta_n, n = 1 - 6$ ; now find  $\gamma_n = k_1 \sin \theta_n$ , and corresponding horizontal wavenumbers  $k_{rn} = k_1 \cos \theta_n$ . Observe though that in Eq.(4) we also need a vertical wavenumber in the lower (seabed) medium, call it  $\gamma_{2n}$ , found via

$$\sin \theta_{2n} = i \sqrt{\left( \frac{c_2}{c_1} \cos \theta_n \right)^2 - 1} \quad (6)$$

Then  $\gamma_{2n}$  equals  $k_2 \sin \theta_{2n}$  where it is understood that  $k_2 = \frac{\omega}{c_2}$ . But since all  $\theta_n$  are by definition less than the critical angle, then  $\sin \theta_{2n}$  is imaginary resulting in the necessary exponential decay in the field in the lower medium for  $z > H$ . It's worthwhile to look back now at Lecture 19, where we first discussed what happens in the seabed for grazing angles less than the critical angle.

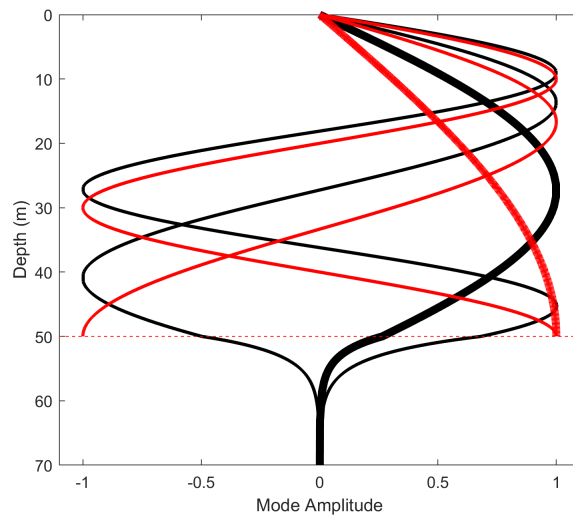


Figure 4: Mode functions for the first three modes finite impedance boundary under discussion in Fig. 3 of this lecture (black lines) compared infinite impedance case (red lines). Mode 1 for each case is plotted with thicker line. Note that for infinite impedance case the mode functions cannot extend below the boundary at depth 50 m.

Examine carefully the mode functions for the first three modes associated with finite impedance boundary case under study (Fig. 4), and compared with equivalent mode functions for the infinite impedance case. With finite impedance case, you can see clearly the exponential decay into the seabed for depths greater than 50 m (refer to Frisk, Eq. (5.145) for how to compute the mode functions there). For this example it appears that modes 2 and 3 are not too different, but the mode 1 case shows a substantial difference. The Green's function so defined by Eq. (5), with  $A_n$  given by Eq.(4) is actively used in underwater acoustics research today; it describes what is known as the Pekeris waveguide, named after the physicist C. L. Pekeris (1908-1993).

### References

- Frisk, G. V. *Ocean and Seabed Acoustics* (Prentice Hall, Englewood Cliffs, NJ, 1994)  
Z. Y. Zang, and C. Tindle, "Complex effective depth of the ocean bottom" *J. Acoust. Soc. Am.* 93,205-213, 1993